Centriolar subdistal appendages promote double strand break repair through homologous recombination

Guillermo Rodríguez-Real[1,2], Andrés Domínguez-Calvo[1,2], Rosario Prados-Carvajal[1,2], Aleix Bayona-Feliú[3], Sónia Gomes-Pereira[4], Fernando R. Balestra[1,2,]*, and Pablo Huertas[1, 2,]*

[1] Departamento de Genética, Facultad de Biología, Universidad de Sevilla, Sevilla, 41080, Spain

[2] Centro Andaluz de Biología Molecular y Medicina Regenerativa-CABIMER, Universidad de Sevilla-CSIC-Universidad Pablo de Olavide**,** Sevilla, 41092, Spain

[3] Genome Data Science, Institute for Research in Biomedicine (IRB Barcelona), The Barcelona Institute of Science and Technology (BIST), Barcelona, 08028, Spain

[4]University of Geneva, Department of Cell Biology, Sciences III, Geneva, Switzerland

*To whom correspondence should be addressed. Tel: +34 954 467 667; Fax: +34 954 461 664; Emails: fernando.balestra@cabimer.es, pablo.huertas@cabimer.es

Fernando R. Balestra ORCID #: 0000-0003-2741-6068

Pablo Huertas ORCID #: 0000-0002-1756-4449

Lead Contact: Pablo Huertas

Abstract

The centrosome is a cytoplasmic organelle with roles in microtubule organization which has also been proposed to act as a hub for cellular signaling. Some centrosomal components are required for full activation of the DNA Damage Response. However, if the centrosome regulates specific DNA repair pathways is not known. Here, we show that centrosomes presence is required to fully activate recombination, specifically to completely license its initial step, the so-called DNA end resection. Furthermore, we identify a centriolar structure, the subdistal appendages, and a specific factor, CEP170, as the critical centrosomal component involved in the regulation of recombination and resection, albeit it does not control end-joining repair. Cells lacking centrosomes or depleted for CEP170 are, consequently, hyper-sensitive to DNA damaging agents. Moreover, low levels of CEP170 in multiple cancer types correlate with an increase of the mutation burden associated with specific mutational signatures and a better prognosis, suggesting that changes in CEP170 can act as a mutation driver but also could be targeted to improve current oncological treatments.

Keywords: DNA end resection/ Homologous recombination/ Centrosomes/ Subdistal appendages/ CEP170

Introduction

The centrosome is considered the major microtubule (MT) organizing center (MTOC) of animal cells, involved in mitotic spindle assembly, interphase MT-network organization and cilia and flagella assembly. Centrosomal defects, either in number or structure, are linked to chromosome missegregation, polarity defects and motility or signaling defects related to the lack of cilia or flagella (Bornens, 2012; Nigg & Raff, 2009). The centrosome is composed of a pair of centrioles surrounded by a structured cloud of proteins known as the pericentriolar material (PCM) (Le Guennec *et al*, 2021). The centriolar structure and its assembly pathway has been conserved throughout evolution (Nabais *et al*, 2020). In humans, they are composed by 9 triplets of MTs distributed in a radial symmetry to form a cylinder of approximately 500 nm long and 200 nm wide. In addition to MTs, from two to three hundred proteins have been estimated to localize to the centrosome (Andersen *et al*, 2003; Jakobsen *et al*, 2011). However, only a minority of them has been described to play a role at the centrosome. For instance, the cartwheel component HsSAS-6 or the kinase PLK4 are required for centriolar duplication, thus the inactivation or depletion of either protein in human cultured cells leads to the inhibition of centriole assembly, rendering the appearance of cells without centrioles as the subsequent divisions go by (Wong *et al*, 2015; Wang *et al*, 2015; Gönczy & Hatzopoulos, 2019). Interestingly, centriole depleted cells can assemble a mitotic spindle and perform mitosis, although with a high rate of chromosome missegregation (Wong *et al*, 2015; Wang *et al*, 2015). These cells without centrioles expend a significant longer time in mitosis which leads to the activation of a p53-dependent pathway that leads to a G1 cell cycle arrest (Meitinger *et al*, 2016; Wong *et al*, 2015; Lambrus *et al*, 2016; Fong *et al*, 2016; Lambrus *et al*, 2015). Other well characterized centriolar proteins are the components of the centriolar appendages, substructures present only in mature centrioles (i.e. those that are at least two cell cycle old). Centriolar appendages protrudes from the distal side of the centriole usually displaying a nine-fold radial symmetry and they are classified into two types depending on their position within the centriole: the distal and the subdistal appendages (Le Guennec *et al*, 2021). Centriolar proteins required to build these structures have been identified including ODF2, CEP128, Centriolin, NDEL1, Ninein and CEP170 as key components required to build the

83 subdistal appendages. From a functional point of view, among other roles, distal
84 appendages are essential for cilia assembly and subdistal appendages are involved
85 in MTs anchoring to the centriole (Hall & Hehnly, 2021).

86 Interestingly, it has been proposed that the centrosome plays also cellular
87 functions not directly related to its MTOC activity. One of these functions involves
88 its role as a signaling platform to regulate several cellular processes such as cell
89 polarization, cell cycle regulation or cell proliferation (Arquint *et al*, 2014).
90 Intriguingly, several components of the DNA damage response (DDR) have been
91 identified at the centrosome as the checkpoint proteins ATM, ATR, Chk1 or Chk2
92 and the repair factors BRCA1, BRCA2 or PARPs (Mullee & Morrison, 2016).
93 Additionally, several centrosomal proteins have been shown to play a direct role in
94 specific DNA damage repair pathways, for example Centrin-2 in nucleotide
95 excision repair (Dantas *et al*, 2011), or PCNT and CEP164 in checkpoint triggering
96 by ATR and ATM activation (Sivasubramaniam *et al*, 2008; Griffith *et al*, 2008),
97 although the role of CEP164 in DNA repair has been recently disputed (Daly *et al*,
98 2016). However, it remains unclear if and how the centrosome itself plays a role
99 specifically in the regulation of the DNA double strand breaks (DSBs) repair
100 pathways.

101 DSBs are one of the most challenging DNA lesions to be fixed. As the rest of
102 DNA damage, they can arise due to exposure to exogenous (chemicals, irradiation,
103 etc.) or endogenous (transcription or replication problems) (Ciccia & Elledge,
104 2010; Tubbs & Nussenzweig, 2017; Jackson & Bartek, 2009). In contrast to other
105 DNA lesions, DSBs lack an intact DNA strand to use as a template during repair,
106 hence they are particularly complex to repair. Indeed, DSBs appearance triggers a
107 complex response, the already mentioned DDR, which overhauls the whole cellular
108 metabolism. The DDR is triggered mainly by the activation of the kinases ATM,
109 ATR, Chk1 and Chk2 (Blackford & Jackson, 2017; Ciccia & Elledge, 2010), in a
110 complex process that, as mentioned, requires partially centrosomal components
111 (Mullee & Morrison, 2016). Furthermore, DSBs could be repaired by using one out
112 of several possible mechanisms that can be grouped in two major families: the
113 homologous recombination pathways (HR) or the non-homologous end-joining
114 pathway (NHEJ) (Chang *et al*, 2017; Ranjha *et al*, 2018; Jasin & Rothstein, 2013).
115 Upon the detection of a DSB, the cell needs to commit to one of these two

116 alternative repair pathways, and the outcome of the repair in terms of fidelity is
117 dependent on this decision. The choice is influenced by different cellular cues, such
118 as cell cycle stage. HR can almost only be executed after DNA replication (in S and
119 G2 phases) when the sister chromatid is present and can be used as a template to
120 repair the damaged molecule (Symington, 2016; Jasin & Rothstein, 2013). On the
121 contrary, NHEJ that relies on the ligation of the two ends of DNA with little
122 processing and without a template, can be performed through the whole cell cycle
123 (Chang *et al*, 2017). A complex molecular network is involved in determining the
124 repair pathway of choice (HR vs. NHEJ) upon the detection of a DSB, thus affecting
125 DSB repair outcome. Nevertheless, it happens mostly by controlling the initial step
126 of HR, the so-called DNA end resection (Cejka, 2015; Symington, 2016). This
127 consists in the extensive processing of the DNA ends by nucleases to form long tails
128 of 3' OH protruding long tails of single stranded DNA (ssDNA). These ssDNAs are
129 initially coated by the RPA complex (RPA1, RPA2, and RPA3), which protects it
130 from degradation and from pairing with other ssDNAs. Importantly, resected DNA
131 effectively blocks NHEJ, hence committing the repair through HR. Mostly, cellular
132 cues that promote the licensing of DNA end resection, thus promoting HR, affect
133 the activation of the nuclease activity of the MRN complex (MRE11-RAD50-NBS1)
134 through the regulation of CtIP and its partner BRCA1 (Symington, 2016; Cejka,
135 2015). This triggers the so-called short-range DNA end resection that is followed
136 by a more extensive resection, known as long-range resection (Symington, 2016;
137 Cejka, 2015). From that point onward, HR can happen by different means in a
138 complex molecular choreography that ends with the use of a homologous template
139 for repair (Jasin & Rothstein, 2013). Among other factors, it usually requires the
140 recruitment of the recombinase Rad51 that modulates the invasion of the
141 homologous template.
142
143 Interestingly, among the proteins identified to localize to the centrosome, in
144 addition of proteins involved in the DDR (such as ATM, ATR, Chk1 or Chk2) there is
145 a subgroup of them linked directly to DSBs repair by HR (i.e. BRCA1 and BRCA2).
146 Thus, we wondered whether the centrosome might play a direct role in HR and,
147 more specifically, in regulating the choice between this repair mechanism and
148 NHEJ by affecting DNA end resection. Strikingly, we observed that cells without

149 centrioles are defective in DNA end resection and HR, supporting this hypothesis.
150 Moreover, such regulation of DNA end resection at centrioles relies on the
151 subdistal appendages. We found that phosphorylation of the subdistal appendage
152 protein CEP170 by the checkpoint kinases ATM and ATR is required to fully
153 activate HR pathway. In the absence of centrioles, subdistal appendages or
154 CEP170, HR is defective, rendering cells hyper-sensitive to DNA damaging agents.
155 Strikingly, CEP170 levels are altered in several tumors. Interestingly, low levels of
156 the protein increase their mutational burden with specific mutational signatures,
157 chiefly among them the one associated with HR defect. Furthermore, low levels of
158 CEP170 levels correlates with poorer cancer prognosis.
159
160 **Results**
161 <u>The centrosome promotes the repair of DNA Double Strand Breaks through</u>
162 <u>homologous recombination.</u>
163
164 Despite the aforementioned connection between the centrosome and the DDR, it is
165 unknown if there is a direct centrosomal role on DSB repair pathway choice.
166 Intrigued by this possibility, we generated U2OS cells without centrosomes using
167 the PLK4 inhibitor centrinone (Wong *et al*, 2015). As mentioned, PLK4 activity is
168 required for centriole duplication, thus its inhibition leads to cells that while
169 dividing in subsequent cell cycles dilute their preexisting centrioles rendering to
170 the appearance of centrosome-less cells in the population. Centriolar loss requires
171 therefore several cell divisions, hence cannot be observed upon short treatments
172 but only after exposure to the drug for several days (see Figure EV1A and B
173 comparing the 1 day *vs* 7 days time points). We then used this condition to test the
174 impact of centriole loss on the balance between NHEJ and HR repair pathway
175 choice (Figure 1A-B). We used a duo of stably transfected GFP-based repair
176 reporters in which the ectopic expression of the I-SceI nuclease fused to BFP (Blue
177 fluorescent protein) triggers the reconstitution of an active GFP when a specific
178 repair pathway, either HR or NHEJ, is activated (Pierce *et al*, 1999; Bennardo *et al*,
179 2008) (Figure 1A-B). In this experimental set up, infection efficiency for all
180 conditions were monitored and only BFP positive cells were taken into
181 consideration for GFP analysis (for more details see Material and Methods).

182 Strikingly, centriole depleted cells, i.e. treated with centrinone for 7 days,
183 compromised the homologous recombination Rad51-dependent gene conversion
184 pathway (Figure 1A) and at the same time promoted the error prone NHEJ repair
185 (Figure 1B), suggesting that indeed centrosomes are critical to balance DSB-repair
186 pathway choice. As introduced, this decision occurs usually by regulating HR, and
187 mostly by licensing or not DNA end resection. To dissect at which step the
188 centrosome impinges on this process, we monitored by immunofluorescence key
189 steps of the homologous recombination repair pathway. Specifically, we inspected
190 the steps of DNA end resection (RPA foci), of HR initiation/commitment (BRCA1
191 foci), and strand invasion for HR (RAD51 foci) in U2OS cells depleted for centrioles
192 and challenged with 10Gy of ionizing radiation. Centrosome depleted cells showed
193 a significant drop in all three steps of HR (Figure 1C-E) suggesting that
194 centrosomes are required to activate HR from the earliest step, i.e. affecting
195 already the licensing of DNA end resection. Similar resection impairment was
196 observed in centrinone treated U2OS cells when DNA damage was induced by
197 Camptothecin (Figure EV1C) or in centrinone treated RPE-1 cells irradiated with
198 10 Gy (Figure EV1D). To discard that centrinone itself could directly have an effect
199 in HR independently of its effect on centriole duplication, we repeated the RPA foci
200 formation experiment in cells treated with centrinone but only for one day, thus in
201 which the majority of cells retain centrioles, and no impact on resection was
202 observed (Figure EV1E). Finally, to confirm that centriole loss and not extended
203 centrinone treatment by other means impair HR, we repeated the same
204 experimental strategy making use of the HsSAS-6 knock out RPE-1 p53-/- cell line.
205 HsSAS-6 is an essential protein for centriole duplication and therefore HsSAS-6 KO
206 cells are devoid of centrosomes and they are only viable in the absence of p53
207 (Wang *et al*, 2015; Leidel *et al*, 2005). In agreement with our previous results,
208 HsSAS-6 KO p53 -/- cells also showed a significant decrease in resection compared
209 to control RPE-1 p53 -/- cells (Figure EV1F).

210 Since all our data supported a role of the centrosome as a regulator of HR,
211 we wondered whether this regulation relied on its presence/absence or the
212 number of centrosomes. Thus, we wondered if cells bearing an excess number of
213 centrosomes could also display an imbalance in HR *vs.* NHEJ. To test this idea, we
214 transiently overexpressed an mCherry-tagged version of PLK4 (Moyer *et al*, 2015)

215 which leads to ~35% of cells bearing extra centrosomes in our cell population
216 (Figure EV1G). Notably, we could not observe any imbalance between HR *vs.* NHEJ
217 in this condition (Figure EV1H and I) suggesting that presence or absence, but not
218 number of centrosomes regulates double strand break repair pathway choice.
219 We wonder if centrosome lost itself could induce DNA double strand breaks. To
220 test this idea, we used the phosphorylated form of the histone variant H2AX
221 (γH2AX) as a marker of DSB. As expected, we did not observe any impact on γH2AX
222 foci formation upon centrinone treatment (Figure EV1J). We then checked whether
223 the imbalance observed in centrosome depleted cells between the two main
224 double strand break repair pathways would eventually lead to a delay or a lack of
225 repair or if it will simply result on a switch between HR and NHEJ. To do so, we
226 compared the foci dynamics of γH2AX for 6 hours after irradiation in control and
227 centriole depleted cells (Figure EV1K). Notably, we did not observe any significant
228 change in the dynamics of chromosome break repair in centriole depleted cells,
229 supporting the idea that the decrease of double strand break repair by HR is
230 countervailed by an increase in NHEJ repair pathway (Fig. 1A and 1B). Intriguingly,
231 we did not observe an overall increase on NHEJ regulators, such as RIF1 nuclear
232 foci, in irradiated centriole depleted cells (Figure EV1L). If any, we observed a
233 slight reduction on RIF1 accumulation. As RIF1 is an accessory NHEJ factor
234 involved in counteracting resection, our data argue that the increase in NHEJ
235 observed in acentriolar cells does not simply rely on hampering DNA end
236 processing. We then wondered about the mechanism by which the centrosome
237 could be regulating HR *vs.* NHEJ repair pathway choice. We hypothesized that the
238 role of the centrosome in DSB repair might rely on its activity as a microtubule
239 nucleator during interphase. To test this, we measured resection in irradiated
240 U2OS cells pretreated either with MTs depolymerizing (Nocodazole) or stabilizing
241 (Taxol) drugs (Figure EV1M). Neither of the two treatments mimicked the impact
242 of centrosome loss, suggesting that the connection of the centrosome with DSB
243 repair is independent of its MTOC activity. Overall, we concluded that by a so far
244 uncharacterized mechanism, the centrosome promotes DNA DSB repair by
245 stimulating homologous recombination and impairing NHEJ in a fashion that is
246 independent of its MT organization function.
247

248 <u>DNA double strand break repair imbalance upon centrosome loss is not a</u>
249 <u>consequence of cell cycle perturbance.</u>
250
251 Notably, extended centrinone treatment has been reported to prolong mitosis
252 through a 53BP1-USP28-mediated activation of p53 and p21, which eventually
253 blocks the cell cycle in G1 (Meitinger *et al*, 2016; Wong *et al*, 2015; Fong *et al*,
254 2016; Lambrus *et al*, 2016). As cell cycle is a major regulator of DNA end resection
255 and HR (Huertas, 2010), we wondered if such response could account for the
256 imbalance observed in DNA double strand break repair. Interestingly, in our
257 experimental conditions, we did not observe either a significant accumulation in
258 G1, an increase of mitotic cells or cell death in cells treated with centrinone (Figure
259 EV1N-Q). Moreover, our results in HsSAS-6 KO cells were already obtained in a
260 p53 KO background, reinforcing the idea that this effect was cell cycle independent
261 (Figure EV1F). Despite that, to further rule out that the absence of centrosomes
262 could be modulating HR indirectly through changes in cell cycle progression
263 mediated by p53, we performed similar experiments in not only Saos-2 cells, a
264 primary osteosarcoma p53-/- cell line, but also in RPE-1 lacking either p53 or p21
265 (Hauge *et al*, 2019). We obtained similar results to the ones observed in U2OS and
266 RPE-1 cells with all cell lines (Figure EV1R-Z), supporting the idea that the effect of
267 centriolar loss on HR is independent of an accumulation in G1 or mitosis. However,
268 HR takes place during S and G2, and centrinone treatment increases the number of
269 cells in G2 (Figure EV1N). Although we already observed that treatment with
270 camptothecin, that specifically creates DSBs at S phase, was compromised upon
271 centrinone treatment (Figure EV1C), we tested if centriole loss affected equally
272 DNA end resection in these both phases of the cell cycle by using quantitative
273 image-based cytometry (QIBC) upon irradiation (Figure 1F-H). With this approach,
274 we measured DNA content (DAPI intensity), active DNA replication (with an EdU
275 pulse) and DNA resection (through RPA foci), by fluorescent microscopy (Figure
276 1F-H). As expected, no resection was observed in G1 cells in any condition.
277 Furthermore, this analysis confirmed that the decrease in resection upon
278 centrinone treatment is similar in both S and G2 phases.
279

280 Centriolar subdistal appendages proteins promote DNA end resection after double
281 strand break.
282
283 As stated in the introduction, a few DDR and HR proteins are located at the
284 centrosome (ATM, ATR, CHK1, CHK2, BRCA1, BRCA2) and some centriolar proteins
285 have been previously involved in DDR (Centrin2, CEP63, PCNT) (Mullee &
286 Morrison, 2016; Dantas *et al*, 2011; Sivasubramaniam *et al*, 2008; Alderton *et al*,
287 2006), suggesting a close crosstalk between them. We envisaged that the
288 regulation of DSB repair pathway choice by centrosomes will require one or
289 several proteins sharing either of these characteristics: a DDR protein that resides
290 temporarily at the centrosome or a centrosomal-factor that regulates and/or is
291 regulated by the DDR. To search for these factors with an unbiased approach we
292 decided to retrieve previously published data from several publications and
293 databases of either DNA repair/DDR/DDR-regulated factors or
294 centriole/centrosome associated proteins and performed an *in silico* metanalysis
295 to look for common factors within these two categories. This metanalysis retrieved
296 a list of genes previously connected to DDR (1457 genes) and to centrosome
297 biology (1424 genes). The cross-check of these two lists led to the identification of
298 159 genes linked to both processes (Figure 2A; Figure EV2A; Table EV1). Among
299 these 159 genes, caught our attention a group of 3 genes previously reported to be
300 part of a very defined substructure of the centrioles, the subdistal appendages
301 (CEP128, NIN and CEP170) (Hall & Hehnly, 2021). A handful of proteins have been
302 identified to be part of such structure: ODF2, CEP128, Centriolin, NDEL1, Ninein
303 and CEP170. Their architecture follows a hierarchical organization with ODF2 at
304 the root, and the most proximal to the centriole wall. From that point the structure
305 branches, with a short bough formed by NDEL1 and a second longer one formed by
306 Cep128-Centriolin-Ninein and CEP170, in that order from the inner part to the
307 periphery (Figure 2B). To assess whether the subdistal appendages as a structure
308 is involved in DSB repair, and most specifically in activating HR by licensing DNA
309 end resection, we depleted the above-mentioned proteins using siRNA against
310 them. Depletion of these components was confirmed either by western blot or by
311 RT-PCR, depending on the availability of specific antibodies (Figure EV2B-D).
312 Interestingly, while reduction of ODF2, Centriolin, Ninein and CEP170 showed a

313 significant drop in DNA end resection after DNA damage, albeit to different extents,
314 depletion of NDEL1 did not have a significant impact on the process (Figure 2C).
315 Knockdown of the core resection factor CtIP was used as a positive control. Thus,
316 we conclude that the subdistal appendages, at least the longer branch, is required
317 for fully activation of DNA end resection. Intrigued by these results, we reasoned
318 that the most peripheral component of the long branch of the subdistal
319 appendages, CEP170, could be the critical factor involved in DNA end processing.
320 Therefore, the effect of the depletion of other subdistal appendages proteins might
321 reflect their impact on CEP170 localization to this centriolar structure. To test this
322 idea, we quantified CEP170 levels at the centrosome after depletion of all the
323 subdistal appendages proteins using the same samples that were used for RPA foci
324 formation (Figure 2D). As published, depletion of ODF2, CEP128, Centriolin and
325 Ninein, but not NDEL1, affected CEP170 localization at centrioles to different
326 extents. As expected, downregulation of the core resection factor CtIP did not affect
327 this localization either. Strikingly, and in agreement with our hypothesis, we found
328 a correlation between the decrease of CEP170 levels at the centrosome and the
329 drop on DNA end resection (Figure 2E; R^2=0.9799). Furthermore, this drop in DNA
330 end resection was also confirmed in the RPE-1 CEP128 KO cell line (Mönnich *et al*,
331 2018) where CEP170 levels at the centrosome is also partially reduced (Figure
332 EV2E-F). CEP170 depletion phenotype was rescued by a siRNA-resistant version of
333 the gene (Figure 2F and Figure EV2G). Moreover, the drop in DNA end resection
334 after CEP170 depletion was also observed when cells were challenged with the
335 DNA damaging agent Camptothecin (Figure EV2H). We also confirmed that
336 CEP170 depletion itself has no impact on RPA or γH2AX foci formation in the
337 absence of an exogenous source DNA damage (Figure EV2I-J). Lastly, we used
338 CRISPR/Cas9 technique to create a KO of CEP170 in RPE cells. Unfortunately, we
339 were not able to recover a full KO, suggesting the protein is essential. However, we
340 created several independent heterozygous CEP170 +/- modified cell lines (Figure
341 EV2K). All those heterozygous cell lines for CEP170 also displayed a clear drop in
342 DNA end resection (Figure 2G). All together, these results revealed that the
343 subdistal appendages are key structures within the centriole involved in DNA end
344 resection and point to CEP170 as the critical mediator of this process.
345

346 CEP170 promotes homologous recombination from the centrosome.

347

348 Our data suggest that the subdistal appendage component CEP170 promotes DNA
349 end resection after DSB damage, and this DNA processing requires the presence of
350 centrioles. To link those two observations, and test if CEP170 was affecting
351 resection from the centrosome and not due to a putative, unknown, centrosome-
352 independent function, we tested the effect of CEP170 depletion on DNA end
353 resection in cells without centrioles. As control, we performed similar experiments
354 depleting the HR regulator CtIP. Interestingly, we observed that while CtIP
355 depletion in cells without centrioles further reduced DNA end resection, depletion
356 of CEP170 in cells without centrioles did not show any impact (Figure 3A), thus
357 suggesting that the loss of centrioles is epistatic over CEP170 role but not over a
358 core resection protein such as CtIP. Therefore, the lack of an additive phenotype in
359 centriole-less cells depleted of CEP170 strongly support that CEP170´s role in DDR
360 is played from the centrosome. Furthermore, as the absence of centrioles and the
361 depletion of CEP170 rendered similar resection defect, our data also favors that
362 CEP170 might be the main centrosomal factor accounting for the centrosomes' role
363 in resection. We then considered that even if CEP170´s role in DDR might require,
364 initially, a centrosomal localization, a possible scenario could be that CEP170
365 might delocalize to DNA after damage and play a direct role in HR within the
366 nucleus or even at sites of DNA damage. However, an ectopically expressed version
367 of CEP170 tagged with GFP neither relocalized to the nucleus nor was recruited to
368 laser micro-irradiated DNA damage (unpublished observations). Furthermore,
369 CEP170 protein distribution nucleus vs. cytoplasm was also not altered upon
370 irradiation (Figure EV3A), supporting an indirect role of CEP170 in HR repair
371 pathway from the centrosome.

372

373 So far, we have shown that the centrosome is required for a proper balance
374 between HR and NHEJ, affecting both repair pathways, and that it specifically
375 regulates the initial step of HR, DNA end resection. Also, that the subdistal
376 centriolar protein CEP170 plays a critical role in DNA processing activation. To
377 study whether the role of CEP170, as this of centrosomes, extend not only to DNA
378 end resection but also to both HR and NHEJ, we analyzed the ability of CEP170

379 depleted cells to perform different types of DSB repair using the GFP-based
380 reporters described above. In agreement with a role in DNA end resection,
381 homologous recombination Rad51-dependent gene conversion pathway was
382 compromised (Figure 3B). On the other hand, and in stark contrast with our
383 observation in centrosome-less cells, no significant impact on the NHEJ repair
384 pathway was observed (Figure 3C). In addition to the above-mentioned drop of
385 RPA foci in CEP170 depleted cells after irradiation, we also observed a drop of
386 BRCA1 or Rad51 foci (Figure 3D and 3E) and a small but significant reduction on
387 the recruitment of the NHEJ facilitator RIF1 (Figure 3F) along the same lines to the
388 observed changes upon centrinone treatments. Similar changes were observed in
389 CEP128 KO RPE1 cells (Figure EV3B-C). All together our data supports that
390 CEP170, and the SDA, plays a critical role on the centriole subdistal appendages-
391 based regulation of HR. It also suggests that the increase on NHEJ observed in cells
392 lacking centrosomes must be mediated by an additional, yet undiscovered,
393 centriolar factor.
394
395 CEP170-S637 phosphorylation modulates DNA end resection.
396 We then wondered about the molecular steps that might connect DSBs
397 repair and CEP170´s role in HR. Neither cytoplasmic CEP170 protein levels nor
398 overall CEP170 levels changed after irradiation-induced DNA damage (Figure
399 EV3A and D). Remarkably, CEP170 was previously identified in a large-scale
400 proteomic analysis of proteins phosphorylated in response to DNA damage on a
401 consensus site recognized by ATM and ATR (Matsuoka *et al*, 2007). Specifically,
402 Serine-637 of CEP170 is an evolutionary conserved site in vertebrates (Figure
403 EV3E) identified as a residue phosphorylated after DNA damage (Matsuoka *et al*,
404 2007). To assess if this putative phosphorylation site is biologically relevant, we
405 generated mutated versions of CEP170 either mimicking (CEP170-S637D) or
406 disrupting this phosphorylation (CEP170-S637A) (Figure EV3F). We confirmed by
407 Ultrastructure Expansion Microscopy (U-ExM) that both mutated versions of
408 CEP170 tagged to GFP, when expressed ectopically, showed a similar localization
409 to the subdistal appendages and the proximal side of the centriole as the one
410 reported for the endogenous protein or the also ectopically expressed wildtype
411 version of GFP-tagged CEP170 (Figure 3G). Only in a minority of cells, but

412 regardless of the version of the protein expressed, the overexpression of the
413 protein rendered the accumulation in additional centrosomal locations (Figure
414 EV3G). Thus, we concluded that this expression of different CEP170 species can be
415 used as a complementation system for the endogenous protein. Interestingly,
416 expression of CEP170-S637D but not CEP170-S637A rescued CEP170-depletion
417 RPA phenotype (Figure 3H), suggesting that not only the presence of the protein,
418 but its phosphorylation, is required to fully activate resection. We hypothesized
419 then that after irradiation, CEP170 is phosphorylated by ATM/ATR in S637 which
420 is critical for promoting HR as the pathway of choice for DSB repair. As expected,
421 the expression of CEP170-S637D alone was unable to rescue the drop of RPA foci
422 formation observed upon chemical inhibition of ATM/ATR (Figure EV3H), in
423 agreement with the fact that CEP170 is just one of many targets involved in
424 homologous recombination that is phosphorylated by ATM/ATR in response to
425 DNA damage. As our results support that CEP170´s role in HR is centrosomal-
426 dependent (Figure 3A), and ATM/ATR have been reported to localize to the
427 centrosome (Mullee & Morrison, 2016), we hypothesized that such
428 phosphorylation happens at that localization. We then wondered whether once
429 phosphorylated, CEP170 function in HR could be centrosome independent. To
430 assess this possibility, we overexpressed the phosphomimic CEP170-S637D
431 mutant in centriole depleted cells. Interestingly, CEP170-S637D did not
432 compensate the drop in HR observed in centriole depleted cells (Figure EV3I).
433 Therefore, we concluded that CEP170 location at the centrosome is most likely
434 required for CEP170 phosphorylation by ATM/ATR and for its subsequent role
435 promoting HR.
436
437 <u>Centrosome/CEP170 DNA damage response contributes to cell survival after DNA</u>
438 <u>double strand break.</u>
439
440 The above-mentioned results reveal a new function of the centrosome and the
441 centriolar protein CEP170 in DSB repair. To assess whether this function
442 contributes to cell survival and proliferation after DNA damage, we performed
443 clonogenic assays with RPE-1 cells either absent of centrioles or heterozygous by
444 CRISPR for CEP170 (Figure EV2K). In agreement with our hypothesis, both

445 conditions rendered cells hypersensitive to DSB-inducing agents such as ionizing
446 radiation (IR), the radiomimetic agent Neocarzinostatin (NCS), or both
447 topoisomerase poisons Camptothecin (CPT) and Etoposide (VP-16) (Figures 4A-H,
448 Figure EV4). These hypersensitivities were of a similar extent to the ones observed
449 for other canonical regulators of HR repair pathway choice such as BRCA1 (Cruz-
450 García *et al*, 2014). Interestingly, CEP170 knockdown, albeit causing a similar
451 reduction on RPA foci and HR as centrinone treatment, rendered a stronger hyper-
452 sensitivity to DNA damaging agents, probably reflecting the lack of stimulation of
453 NHEJ in that condition when compared with centrinone treatment. Notably, this
454 hypersensitivity to irradiation was also observed in CEP170 siRNA depleted cells
455 and could be rescued by expressing the siRNA resistant version of CEP170 (Figure
456 4I-J). We concluded that the role of the centrosomes and specifically the centriolar
457 protein CEP170 in HR DNA repair is critical to ensure cell survival and
458 proliferation upon DNA damage.
459
460 <u>CEP170 in cancer biology and cancer prognosis</u>
461
462 Strikingly, changes in the overall levels of CEP170, either downregulation or
463 upregulation, can be observed in many tumor samples (Figure 5A). So, we then
464 speculated that, considering this newly found role in controlling DNA repair, the
465 levels of this protein might relate with the appearance of specific mutations during
466 cancer progression. In other words, we wondered whether tumor cells with low
467 levels of CEP170 might contribute to the appearance of specific mutational
468 signatures and, furthermore, whether those signatures might correlate with
469 defects in specific DNA repair pathways, mainly with HR defects. Using the Pan-
470 Cancer Analysis of Whole Genomes (PCAWG) (Campbell *et al*, 2020) we found 435
471 tumor samples from which we could obtain and analyze mutations on DNA and
472 CEP170 expression data. Based on CEP170 expression, we divided the samples in
473 four quartiles, from the lowest (Q1) to the highest (Q4) RNA levels. Then, we used
474 the SigProfiler software (Bergstrom *et al*, 2019; Islam *et al*, 2020), and identified
475 16 optimal mutation signatures in our dataset by the trade-off of the mean sample
476 cosine distance and average stability of solutions in the range from 1 to 20 (Figure
477 5B; Figure EV5A; see methods for details). Out of those 16 signatures, 11(names

478 marked in red in Figure 5C-R) showed significant exposure differences between
479 samples with low CEP170 expression (Q1) versus high levels of the protein (Q4),
480 with a general increase in those specific mutation burdens (Figure 5C-R). The
481 composition of the actual mutational signatures can be found in Figure EV5A. Next,
482 we compared our signatures to the Catalogue of Somatic Mutations in Cancer
483 (COSMIC) (Tate *et al*, 2019) reference mutational signatures to infer the potential
484 sources of the observed mutagenesis (Appendix Figure S1). Strikingly, from this
485 comparison, we observed that from the signatures that showed exposure
486 differences in tumor cells expressing lower levels of CEP170, stood out several that
487 were similar to the ones associated with defective DNA repair in COSMIC, and
488 outstandingly the one related with defective HR, (Figure 5I) in agreement with our
489 observation that this protein is required for proficient recombination. Remarkably,
490 expression levels of other subdistal appendages proteins as NIN and Centriolin
491 showed similar mutational signatures to the one of CEP170, including compatible
492 with defective HR (Figure EV5B and Appendix Figure S2). More interestingly, in
493 this case NDEL1 showed a similar pattern but orders of magnitude less statistically
494 significant, whereas CEP128 did not (see discussion).
495
496 As cells depleted for CEP170 were hypersensitive to DNA damaging agents used in
497 chemotherapy (Fig 4A-D), and tumor samples with lower levels of CEP170
498 expression accumulate mutations that are consistent, among other causes, with an
499 HR defect, we hypothesized that the levels of this centrosomal factor might affect
500 the overall survival in cancer patients. In this scenario, low levels of CEP170 could
501 render tumoral cells deficient in HR and, therefore, hypersensitive to anticancer
502 treatments, thus increasing patient survival. Strikingly, we found that this was the
503 case in several tumor types. Indeed, patients with tumors that showed lower levels
504 of CEP170 had a better prognosis when survival was analyzed from patient
505 databases, likely because of a heightened sensitivity to treatment due to an
506 inability to repair proficiently by HR (Figure 6A-L). This suggests that CEP170´s
507 role in HR might be relevant in cancer progression but also its levels might be
508 exploited as a biomarker for cancer treatment response.
509
510 **Discussion**

511 The centrosome is a multifunctional organelle frequently highlighted for its
512 ability to nucleate MTs. Indeed, the more striking consequences of centrioles loss
513 in cell cycle progression is a significant delay in spindle assembly which has been
514 linked to the lack of centrosomal MTOC activity (Wong *et al*, 2015; Fong *et al*,
515 2016; Meitinger *et al*, 2016; Lambrus *et al*, 2016). Additionally, the centriole works
516 as a scaffold to assemble the primary cilia and flagella, a function evolutionary
517 conserved from the last common eukaryotic ancestor (Bornens, 2012). However,
518 the centriole has also been proposed to play roles unrelated to these activities. For
519 instance, in *C. elegans*, after fertilization, the sperm centrioles provide the initial
520 clue to define the anterior-posterior cell axis and trigger the polarization of the one
521 cell stage embryo required for the first asymmetric embryonic division (Portier *et*
522 *al*, 2007; Hachet *et al*, 2007). Similar signaling functions of the centrosome has
523 been reported also in mammalian cells (Arquint *et al*, 2014). Several cell cycle
524 regulators localize to the centrosome (Cdk1/Cyclin B, Cdc25B, Cdc25C, Plk1 and
525 Aurora A), which serve as a regulatory platform for G2/M transition, a process that
526 needs to be coordinated to centrosome maturation in order to assemble the
527 mitotic spindle in proper time (Arquint et al., 2014). An additional example on how
528 the centrosome is involved in a signaling pathway to stop cell proliferation of cells
529 with excess number of centrioles has been reported recently. Such role is mediated
530 in human cultured cells by the distal appendage protein ANKRD26, which in turn
531 facilitates the activation of the PIDD as a protective response in cells with excess
532 number of centrioles (Fava *et al*, 2017; Evans *et al*, 2021). Overall, these roles
533 suggest that the centrosome might work as a signaling hub that receives, integrates
534 and elicits a response to preserve cellular viability and fitness.
535
536 *Role of the centrosome on DNA damage*
537 It has been previously proposed that the centrosome is important for a fully
538 responsive DNA damage response. This hypothesis is sustained by the fact that
539 several DDR proteins have been found at centrosome and some centrosomal
540 components are directly involved in DDR (Mullee & Morrison, 2016). However, if
541 centriole loss impairs a specific DDR pathway has not been tested. Here, we show
542 that the centrosome directly regulates the fate of DSBs by channeling its repair
543 toward specific pathways. This new role of the centriole affects cells in both S and

544 G2 phases and is independent of centrosomal MTOC activity during interphase.
545 Centrosome loss by itself leads to a bias in DSBs repair towards NHEJ, upregulating
546 this error prone pathways and impairing the more error-free repair by HR. Indeed,
547 overall DSBs repair, measured by γH2AX foci disappearance, was not affected,
548 arguing that the centrosome promotes quality but is not required for the quantity
549 of the repair. Interestingly, such effect does not simply relay on hampering DNA
550 end resection, as the recruitment of the resection antagonist RIF1 protein is not
551 increased, thus suggesting a more active regulatory pathway at play. Despite that,
552 such change in the repair quality is, indeed, relevant for cell fitness, as centriole
553 depleted human cells were hypersensitive to DNA damaging drugs. Remarkably,
554 this hypersensitivity was not observed on genetically modified DT-40 chicken cells
555 depleted of centrioles (Sir *et al*, 2013). The use of drugs targeting centriole
556 duplication has been suggested before for certain types of tumors as breast
557 cancers or gliomas that overexpress TRIM37. Cells from these types of tumors are
558 hypersensitive to centrosome loss (Meitinger *et al*, 2020; Yeow *et al*, 2020).
559 Considering our data, we propose that the same logic could be applied for the
560 treatment of other tumor types where centrosomal loss could be synergistic with
561 DNA damaging drugs for cancer treatment.
562
563 *The role of CEP170 in the centrosome-mediated regulation of DSB repair*
564 We have been able to identify a particular substructure within the centriole that
565 plays important roles in the regulation of DNA end resection and recombination:
566 the subdistal appendages. More specifically, the part that branches from the
567 centriole from CEP128 and finishes at CEP170. Furthermore, we found that among
568 these proteins CEP170 appears as a key factor mediating the response, as the
569 degree of resection defect observed upon depletion of subdistal appendage factors
570 directly correlates with the impairment of the recruitment of CEP170. In addition
571 to its subdistal appendage localization CEP170 also localizes to the proximal side
572 of the centriole. Although we cannot rule out that CEP170 might be playing a role
573 in DDR from its centriolar proximal localization, the fact the depletion of factors
574 that specifically interfere with CEP170 recruitment to the subdistal appendages
575 and not to its proximal localization at the centriole (i.e. ODF2 and CEP128
576 depletion (Hall & Hehnly, 2021)) support the notion that subdistal appendages and

577 more specifically CEP170 from the subdistal appendages are involved in DDR.
578 Subdistal appendages, and specifically CEP170, have previously been involved in
579 MT anchoring to the distal side of the centrioles (Hall & Hehnly, 2021). If this
580 function of CEP170 might be related to its role in DDR is not clear, however we
581 consider this possibility unlikely as drugs impacting MTs dynamics (i.e., Taxol and
582 Nocodazol) did not show DDR defects. Interestingly, a detailed characterization of
583 the behavior of the DSB repair machinery revealed differences between removing
584 the entire centrosome and depleting CEP170. More strikingly, both complete
585 centrosome removal and CEP170 depletion induced a drop of HR, but depletion of
586 CEP170 did not render an increase in NHEJ repair pathway, in stark contrast with
587 cells treated with centrinone. This fact suggests two interesting ideas. First, it
588 reinforces the hypothesis that the upregulation of NHEJ observed upon
589 centrosome loss does not rely on a passive effect due to a resection impairment but
590 rather to an active regulatory process yet to be defined. Therefore, additional
591 centrosomal factors connecting this organelle directly with NHEJ regulation, and
592 independent of the pathway reported in this work, await to be discovered. And
593 second, that CEP170 depletion causes a stronger defect in DSB repair, as the defect
594 in HR is not counterbalanced by an excess in NHEJ, a hypothesis supported by a
595 higher sensitivity to DNA damaging agents. Might other centriolar proteins
596 promote DNA end resection independently of CEP170? We think this is unlikely as
597 treating CEP170 depleted cells with centrinone did not further downregulate HR.
598 Therefore, our data suggest that subdistal appendages through CEP170 is the most
599 relevant pathway that promotes HR for double DNA strand break repair, however
600 still unidentified centrosomal factors might restrict NHEJ repair pathway choice.
601
602 *The centrosome, a DDR signaling hub outside the nucleus.*
603 But how does the centriole and, specifically CEP170, affect a nuclear event such as
604 DNA end resection without being targeted itself to the nucleus? The easiest
605 explanation would be that the centrosome itself acts as a signaling hub. In this
606 scenario, and similarly to what has been proposed for the full activation of the DDR
607 (Mullee & Morrison, 2016), the DNA damage-elicited signal mediated by ATM/ATR
608 is translated to the centrosome, that will integrate this signal with additional cues
609 from the cellular environment. We propose that a second wave of signaling departs

610 from the centrosome towards the nucleus to regulate DSB repair. Indeed, CEP170
611 regulatory function on DNA resection readily requires its phosphorylation by
612 ATM/ATR at Ser367, and the phosphorylated protein acts without leaving the
613 centrosome. Furthermore, phosphorylated CEP170 requires the centrosome to
614 elicit its function on DSB repair, supporting a signaling role of this protein from the
615 centrosome. If these phosphorylation affects centriolar functions of CEP170
616 remains to be tested.
617 But which factor mediates this second wave? An obvious candidate is BRCA1,
618 which is both a DNA end resection modulator and has been shown to be recruited
619 at the centrosomes. In fact, the sensitivity to DNA damaging agents shown by
620 centrinone treatment or CEP170 depletion is similar to the one observed by the
621 canonical HR regulator BRCA1 (Cruz-García *et al*, 2014). Unfortunately, we have
622 not been able to connect changes in BRCA1 dynamics at the centrosome or in the
623 interaction with CEP170 in response to DNA damage. Thus, the link between the
624 resection machinery and CEP170 remains unknown. How this connection works is
625 still under investigation and will be the subject of further works.
626
627 In any case, and based on our results we propose that, as an analogy of how
628 computers work, the centrosome behaves as a cytoplasmic microprocessor we call
629 the Centrosomal Processing Unit (CPU). In this model, the centrosome receives
630 inputs from different ongoing cellular processes, including the presence or not of
631 DSBs, integrate them within a single hub and compute them to exert a response
632 that will feed back to modulate the relevant cellular molecular mechanisms,
633 including the DDR and the DNA repair pathways themselves. Among the different
634 functions that have been assigned to the centrosome, the role of this organelle as a
635 signaling platform might be the least characterized of them all. Specially, in
636 mammalian cells, very little examples and almost no molecular mechanism have
637 been reported to date nailing down this centrosome function (Arquint *et al*, 2014).
638 Furthermore, examples reported so far of centrosome signaling function in
639 mammalian cells are restricted to centriole biology related processes (i.e. centriole
640 number control, centrosome maturation or spindle assembly) (Arquint *et al*, 2014;
641 Fava *et al*, 2017; Wong *et al*, 2015). To our knowledge, the data presented here are
642 the first example in mammalian cells of the centrosome itself, and not specific

643 centrosomal factors, acting as a signaling platform in a process totally unrelated to
644 canonical centrosome biology. In the particular case of DSB repair, it is interesting
645 that this process relays, at least in relationship with resection regulation, on
646 subdistal appendages, a centriolar substructure that varies with the cell cycle and
647 that is only present in mature centrioles. This could be potentially used to
648 coordinate the cell cycle stage with the DSB repair pathway of choice.
649
650 *Relevance of the CPU role on DNA repair in human health*
651 Fully processive and accurate DNA repair is a critical issue in maintaining a healthy
652 homeostasis at the cellular, tissular and organismal levels. Indeed, and as
653 aforementioned, less than optimal repair is at the root of several hereditary rare
654 diseases but also contributes to cancer development. So, does the role of the
655 centrosome as the CPU, and specifically its function on DNA repair, contribute with
656 the appearance of such diseases? Strikingly, there is one rare disease that clearly
657 connects both the centrosome and the DNA end resection: Seckel Syndrome. For
658 years it has been puzzling that this form of hereditary osteodysplastic dwarfism
659 can be caused either by mutations in the DDR and resection factors (ATR, CtIP,
660 DNA2) (O'Driscoll *et al*, 2004; Qvist *et al*, 2011; Shaheen *et al*, 2014), but also
661 centrosomal proteins (CPAP, CEP63, CEP152, NIN) (Al-Dosari *et al*, 2010; Dauber
662 *et al*, 2012; Sir *et al*, 2011; Kalay *et al*, 2011). Little was understood on how defects
663 in these two apparently unconnected elements were able to cause the same clinical
664 phenotypes, although it has been proposed that this centriolar elements are
665 related with ATR activation. Now, we speculate that is the role of the CPU in DNA
666 end resection might be what actually links the centrosome and Seckel. In this
667 scenario, this syndrome should be considered a bona fide repair-deficient
668 syndrome, what explains why it is clinically similar to other repair-deficient
669 diseases, and that the alteration of the CPU contribution to resection is what causes
670 the syndrome upon mutations of centrosomal proteins. Indeed, this factor can be
671 affecting directly ATR activation at the centrosome but also indirectly by
672 regulating DNA end resection, as this processing creates the ssDNA that is
673 recognized by and activates ATR (Ciccia & Elledge, 2010). This would be a good
674 model to explain that mutations in NIN (Seckel 6 variant), a protein that here we

675 have shown is required for fully processive DNA end resection, are linked to this
676 syndrome.
677
678 Moreover, this effect in repair of the CPU should be considered in cancer etiology.
679 Alterations of centrosomal proteins can be found in many cancer types (Gönczy,
680 2015). The more straightforward way to explain this connection between
681 centrosomal defects and cancer is through chromosome missegregation due to
682 defective spindle organization. Indeed, albeit centrosomes are not completely
683 required for spindle formation, the chances of aberrant mitosis increase when they
684 are not fully functional. Now, we propose that in an additional layer, defective
685 centrosomes not only can affect the appearance of chromosomal instability, but
686 also can affect genetic stability through its role as the CPU in the DNA repair. In
687 agreement, cancer samples with lower CEP170 expression consistently show an
688 accumulation of mutations that belong, among others, to mutational signatures
689 associated with defective DNA repair (BER and HR) or associated with exposure to
690 DNA damaging agents (UV, Aristolochic acid). Intriguingly, expression levels of
691 some but not all centriolar proteins involved in CEP170 recruitment to the
692 subdistal appendages also correlate with this group of molecular signatures (i.e.
693 NIN, Centriolin but not CEP128). Furthermore, expression levels of the subdistal
694 appendages component NDEL1, initially not involved in CEP170 recruitment to the
695 centriole, and which depletion in our hands did not impact HR, also showed a slight
696 but significant correlation with mutational signatures associated to defective DNA
697 repair. Altogether, these data reflect that the role of the centriole in DNA repair
698 might be more complex in the context of cancer, and that compensatory
699 mechanisms might be in place when specific factors such as CEP128 are altered.
700 Overall, our data agrees with the idea that the CPU, and specifically CEP170, acts as
701 a critical hub for regulating DNA repair. Thus, a defective CPU, caused by low levels
702 of CEP170, might contribute to cancer progression increasing the mutation burden
703 of the cells. This opens the door to the possibility that CEP170 acts as a tumor
704 suppressor and its mutations might be considered cancer driver mutations. Our
705 data also suggest that centrosomal defects, including reduced CEP170 levels,
706 hyper-sensitize cells to those treatments *in vitro*. Strikingly, this is also supported
707 by the *in silico* analysis of retrospective studies of cancer samples. Thus,

708 considering collectively that induction of DNA DSBs is a first-line therapeutic
709 approach in cancer and the results exposed in this manuscript, we propose that
710 further understanding of the CPU role in DNA repair will open new research lines
711 and therapeutic avenues in oncology.
712
713 **Material and Methods**
714
715 **Cell lines and growth conditions**
716 U2OS and Saos2 cell lines were grown in DMEM (Sigma-Aldrich) and hTERT-RPE1
717 cell lines were grown in F12 (Sigma Aldrich). These media were supplemented
718 with 10% fetal bovine serum (Sigma-Aldrich), 2 mM L-glutamine (Sigma-Aldrich),
719 100 units/ml penicillin, and 100 μg/ml streptomycin (Sigma-Aldrich). For cells
720 expressing GFP or GFP-CEP170 plasmids, standard medium was supplemented
721 with 0.5 mg/ml G418 (Gibco, Invitrogen). hTERT-RPE1 p53-/- cell line was
722 donated by Dr. Rosa Rios' lab. hTERT-RPE1 p53-/- SAS6-/- was kindly gifted by Dr.
723 Tsou (Wang *et al*, 2015). All cell lines tested negative for mycoplasma
724 contamination. hTERT-RPE1 p53-/- CEP170-/+ cell lines were generated by using
725 CRISPR-Cas9 technology. Single cells were seeded in 96-well plates and left to
726 grow prior to characterization and sequencing. When required, cell viability was
727 determined by performing Trypan Blue (Merck) staining. The percentage of cells
728 negative for Trypan Blue (living cells) was automatically quantified by using
729 DeNovix Cell counter (CellDrop FL-UNLTD).
730 To obtain centriole-less cells, media was supplemented with 125nM centrinone
731 (Hy-18682, MCE) for at least 7 days. In clonogenic survival experiments, cells were
732 exposed to centrinone for 7 days prior to seeding cells in 6-well plates. Centrinone
733 was present during all the duration of the assay.
734 For microtubule alteration assays, cells were treated for 1h with 20 μM Taxol and
735 2h with 1 μg/ml Nocodazol prior to ionizing radiation. DMSO was used as control.
736 **siRNAs, plasmids and transfections**
737 siRNA duplexes were obtained from Sigma-Aldrich or Dharmacon (Table EV2) and
738 were transfected using RNAiMax Lipofectamine Reagent Mix (Life Technologies),
739 according to the manufacturer's instructions.

740 The GFP-CEP170 plasmid (Guarguaglini *et al*, 2005) was obtained from Addgene
741 (#41150). siRNA-resistant and GFP-CEP170 S637A and GFP-CEP170 S637D
742 mutant versions were done using QuikChange Lightning Site-Directed Mutagenesis
743 Kit (#210518). pcDNA5 FRT/TO PLK4-mCherry (Moyer *et al*, 2015) was obtained
744 from Addgene (#80269). Plasmid transfection of U2OS cells was carried out using
745 FuGENE 6 Transfection Reagent (Promega) according to the manufacturer's
746 protocol.
747
748 **HR and NHEJ analysis**
749 U2OS cells bearing a single copy integration of the reporters DR-GFP (Gene
750 conversion) or EJ5-GFP (NHEJ) (Pierce *et al*, 1999; Bennardo *et al*, 2008) were
751 used to analyze the different DSB repair pathways. In all cases, cells were plated in
752 6-well plates. One day after seeding, cells were transfected with the indicated
753 siRNA and the medium was replaced with a fresh one 24 h later. The next day, each
754 duplicate culture was infected with lentiviral particles containing I-SceI–BFP
755 expression construct at MOI 10 using 8 μg/ml polybrene in 2 ml of DMEM. Then,
756 cells were left to grow for an additional 24 h before changing the medium for fresh
757 DMEM, and 48 h after siRNA transfection cells were washed with PBS, trypsinized,
758 neutralized with DMEM, centrifuged for 3 min at 600 g, fixed with 4%
759 paraformaldehyde for 15 min, and collected by centrifugation. Then, cell pellets
760 were washed once with PBS before resuspension in 150 μl of PBS. Samples were
761 analyzed with a LSRFortessa X-20 (BD) with the BD FACSDiva Software v5.0.3.
762 Four different parameters were considered: side scatter (SSC), forward scatter
763 (FSC), blue fluorescence (407 nm violet laser BP, Filter 450/40), green
764 fluorescence (488 nm blue laser BP Filter 530/30). Finally, the number of green
765 cells from at least 10,000 events positives for blue fluorescence (infected with the
766 I-SceI-BFP construct) was scored. To facilitate the comparison between
767 experiments, this ratio was normalized with siRNA control. At least three
768 completely independent experiments were carried out for each condition and the
769 average and standard deviation are represented.
770
771 **Clonogenic cell survival assays**

772 To study cell survival after DNA damage, clonogenic assays were carried out
773 seeding 500 cells in 6-well plates in triplicates. The following day, cells were
774 exposed to DNA damaging agents: DSBs were produced by IR or by acute
775 treatment with topoisomerase inhibitor camptothecin (CPT; Sigma), etoposide
776 (VP16; Sigma) or the radiomimetic agent neocarzinostatin (NCS; Sigma). 2 Gy, 4 Gy
777 or mock treated or incubated for 1 h with 0.01, 0.05, or 0.1 μM CPT, 5, 10 or 20 μM
778 VP-16 or vehicle (DMSO) as control. For NCS, cells were exposed for 1 h to 50 and
779 100 ng/ml concentrations or water as control. After two washes with PBS, fresh
780 medium was added, and cells were incubated at 37 °C for 7 days to allow colony
781 formation. Afterward, cells were stained and visualized in the solution of 0.5%
782 Crystal Violet (Merck) and 20% ethanol (Merck). Once the colonies were stained,
783 the remaining solution was removed, and plates were washed with water. The
784 surviving percentage at each dose was calculated by dividing the average number
785 of visible colonies in treated versus control (mock-treated or vehicle-treated)
786 dishes. For rescue experiments, U2OS cells were transfected with GFP-CEP170 or
787 GFP plasmid as described. 24h after plasmid transfection, transfected cells were
788 selected using DMEM supplemented with G418 for 7 days. Cells were then
789 transfected again with siRNA against CEP170 or non-target sequences and 500 and
790 1000 cells were seeded for clonogenic assay in 24-well plates in triplicates. Cells
791 were exposed to ionizing irradiation (1, 2, 4 Gy or mock treated) 48h after
792 transfection and incubated at 37 °C for 10 days to allow cellular growth. The
793 surviving percentage at each condition was then calculated measuring the
794 occupied well area.
795 In both cases, the experiments were repeated in biological triplicates, and each one
796 in technical replicates.
797 **SDS-PAGE and western blot analysis**
798 Protein extracts were prepared in 2× Laemmli buffer (4% SDS, 20% glycerol, 125
799 mM Tris–HCl, pH 6.8) and heated 10 minutes at 100ºC. Proteins were resolved by
800 SDS–PAGE and transferred to nitrocellulose membranes (Amersham, MERCK).
801 Membranes were blocked with Odyssey Blocking Buffer (LI-COR) and blotted with
802 the appropriate primary antibody and infrared dyed secondary antibodies (LI-
803 COR) (Tables EV2). Antibodies were prepared in blocking buffer supplemented
804 with 0.1% Tween-20. Membranes were air-dried in the dark and scanned in an

805 Odyssey Infrared Imaging System (LI- COR), and images were analyzed with Image
806 Studio software (LI-COR). Cellular fractionation was performed following
807 literature protocols (Gillotin et al., 2018).
808
809 **Immunofluorescence and microscopy**
810 Cells were treated with ionizing radiation or mock treated and incubated. The
811 specific ionizing radiation dose and incubation times are described in each
812 experiment. Then, coverslips were washed once with PBS. The fixation step of the
813 immunofluorescence differs depending on the protein to be visualized. For RPA
814 and BRCA1 foci cells were treated with pre-extraction Buffer (25 mM Tris–HCl, pH
815 7.5, 50 mM NaCl, 1 mM EDTA, 3 mM $MgCl_2$, 300 mM sucrose, and 0.2% Triton X-
816 100) for 5 min on ice and fixed with 4% paraformaldehyde (w/v) in PBS for 15
817 min. For γH2AX, cells growing on coverslips were treated for 10 min on ice with
818 methanol. For RIF1 and RAD51 foci, cells were fixed with 4% paraformaldehyde
819 (w/v) in PBS for 15 min and treated with 0,2% PBS-Triton X-100. Finally, for
820 centrosomal proteins visualization 10 min fixation with methanol at -20ºC was
821 performed. In all cases, after two washes with PBS, cells were blocked for 1 h with
822 5% FBS in PBS, co-stained with the appropriate primary antibodies (Table EV2) in
823 blocking solution overnight at 4 °C or for 2 h at room temperature, washed again
824 with PBS and then co-immunostained with the appropriate secondary antibodies
825 (Table EV2) in blocking buffer. After washing with PBS and dehydrating the
826 samples with ethanol 100%, coverslips were mounted into glass slides using
827 Vectashield mounting medium with DAPI (Vector Laboratories). Samples were
828 visualized and acquired using Leica AF6000 fluorescence microscope or a Leica
829 DMI8 Thunder fluorescence microscope. The analysis of the number of foci
830 formation in all cases was performed automatically using FIJI software and a Fiji
831 custom macro.
832
833 **Ultrastructure expansion microscopy (U-ExM)**
834 Ultrastructure expansion microscopy was performed as described by (Gambarotto
835 *et al*, 2019). Briefly, samples were co-immunostained with antibodies against
836 CEP170 or GFP and a combination of antibodies against alpha and beta tubulin. For
837 imaging, samples were mounted in a poly-D-lysine pre-treated 25 mm coverslip.

838 For image acquisition a Leica DM18 Thunder fluorescence microscope using a
839 100x oil-immersion objective was used. Images were deconvoluted and brightness
840 and contrast were adjusted to improve data visualization.
841
842 **Cell cycle analysis**
843 Cells were fixed with cold 70% ethanol overnight, incubated with 250 µg/ml
844 RNase A (Sigma) and 10 µg/ml propidium iodide (Fluka) at 37 °C for 30 min and
845 analyzed with a LSRFortessa X-20 (BD). Cell cycle distribution data were further
846 analyzed using ModFit LT 5.0 software (Verity Software House Inc).
847
848 **Quantitative image-based cytometry (QIBC).**
849 QIBC protocol was adapted from (Michelena & Altmeyer, 2017). Centrinone
850 treated or control cells were grown in DMEM medium supplemented with EdU (10
851 µM) for 30 minutes and irradiated with 10Gy one hour before fixation. Cells were
852 then washed with PBS, treated with pre-extraction buffer and fixed in A 3.6%
853 paraformaldehyde for 15 minutes at room temperature. Cells were then incubated
854 in 0.5% Triton X-100 in PBS for 15 min, in 2% BSA in PBS for 5 min and in Reaction
855 Cocktail solution (50 mM Tris-HCl, pH 7.5, 150 mM NaCl, 25 mM Cooper reactive,
856 Alexa FluorTM 488 Azide ThermoFisher A10266, and 62.38 mM L-Ascorbic Acid)
857 for 30 minutes. Three consecutive washes with 3% BSA in PBS, wash buffer (0.5
858 mM EDTA in PBS) and PBS 1x was performed before 1h incubation with blocking
859 buffer (3% BSA, 0,1% Tween in PBS). Samples were immunostained with RPA
860 antibodies as described above. Image acquisition was performed with a Leica
861 DM18 Thunder fluorescence microscope using a 63x oil-immersion objective. A
862 single merged image per condition, containing over 5000 cells, was acquired under
863 non-saturating conditions maintaining the settings across all samples within each
864 biological replica. FiJi software was used to detect nuclei and quantify DAPI and
865 EdU intensity per single cell nucleus and used for the identification of each cell
866 cycle phase. RPA foci number per nucleus was automatically determined using a
867 FiJi custom macro, identifying RPA positive cells as those with more than 15 foci on
868 irradiated cells.
869
870 **RNA isolation, reverse transcription and quantitative PCR**

871 RNA extracts were obtained from cells using NZY Total RNA Isolation kit (Nzytech)
872 according to manufacturer's instructions. RNA concentration was quantified by
873 measuring 260 nm absorbance using a NanoDrop DeNovix DS-11 FX
874 spectrophotometer. To obtain complementary DNA (cDNA), 1 μg RNA was
875 subjected to RQ1 DNase treatment (Promega) prior to reverse transcription
876 reaction using Maxima H Minus First Strand cDNA Synthesis kit (Thermo
877 Scientific) according to manufacturer's instructions. Quantitative PCR from cDNA
878 was performed to corroborate siRNA-mediated knockdown of several proteins.
879 For this, iTaq Universal SYBR Green Supermix (Bio-Rad) was used following
880 manufacturer's instructions. DNA primers used for qPCR are listed in Table EV2.
881 qPCR was performed in an Applied Biosystem 7500 FAST Real-Time PCR system.
882 The comparative threshold cycle (Ct) method was used to determine relative
883 transcript levels (Bulletin 5279, Real-Time PCR Applications Guide, Bio-Rad), using
884 β-actin expression as internal control. Expression levels relative to β-actin were
885 determined with the formula $2^{-\Delta\Delta Ct}$ (Livak & Schmittgen, 2001).
886
887 **Bioinformatic analysis and data processing**
888 Literature search was performed to obtain different list of genes related to DDR or
889 centriole processes. Both peer-reviewed publications and databases were used
890 (Van Dam *et al*, 2013; Balestra *et al*, 2013; Alves-Cruzeiro *et al*, 2014; Gerdes *et al*,
891 2009; Kim *et al*, 2010; Li *et al*, 2004; Jakobsen *et al*, 2011; Andersen *et al*, 2003;
892 López-Saavedra *et al*, 2016; Milanowska *et al*, 2011; Arcas *et al*, 2014; Prados-
893 Carvajal *et al*, 2021; Matsuoka *et al*, 2007) as sources for these lists. Knime
894 software was used for the processing and generation of a unique list of DDR-
895 related genes; the same was implemented with centriole-related genes. These two
896 lists were cross checked, generating a list of genes linked to both processes (Table
897 EV1).
898
899 Survival plots and gene expression profiles plots in different cancer types with
900 different CEP170 expression were collected from the web-based tool GEPIA (Gene
901 Expression Profiling Interactive Analysis), with open access in:
902 http://gepia.cancer-pku.cn/index.html.
903

904 Tumor mutation calls were retrieved from the PCAWG resource, containing
905 2,658 whole-cancer genomes and their matching normal tissues across 38 tumor
906 types (The ICGC/TCGA Pan-Cancer Analysis of Whole Genomes Consortium,
907 Nature, 2020). To identify mutational signatures, we considered only single
908 nucleotide variants (SNVs). A total of 21628933 SNVs were used to generate a
909 matrix counts of the SBS96 contexts using the SigProfilerMatrixGenerator
910 software(Bergstrom *et al*, 2019). Mutational signatures and its COSMIC reference
911 similarity were inferred via the non-negative matrix factorization algorithm
912 implemented in the SigProfilerExtractor software (Islam *et al*, 2020). Finally, we
913 selected those samples that also contained expression data (435), divided them
914 into quartiles of CEP170 expression and plotted mutational signature activities
915 corresponding to the first quartile (Q1; low) and fourth quartile of expression (Q4;
916 high) as boxplots using Rstudio (RStudio Team, 2022).
917
918 **Statistical analysis**
919 Statistical significance was determined with a Student's t-test or ANOVA as
920 indicated using PRISM software (Graphpad Software, Inc.), except for mutational
921 signature activities comparisons between low and high CEP170 expression were
922 Wilcoxon test was applied using Rstudio (RStudio Team, 2022). Statistically
923 significant differences were labeled with one, two, three or four asterisks for $p <$
924 0.05, $p < 0.01$, $p < 0.001$ or $p < 0.0001$, respectively.
925
926 **Data Availability**
927 No data related with this project has been deposited in a public database. Original
928 microscopy Images can be found at BioImage Archive
929
930 **ACKNOWLEDGEMENTS.**
931 We thank Maikel Castellano-Pozo and Sonia Jimeno for critical reading of the
932 manuscript. We thank CABIMER microscopy facility and Dr. Paloma Domínguez for
933 her technical support in image acquisition and processing. This work was funded
934 by the R+D+I grant US-1255532 Proyectos I+D+i FEDER Andalucía 2014-2020
935 from the Junta de Andalucía, the grant P18-RT-1204 from the Consejería de
936 Transformación Económica, Industria, Conocimiento y Universidades, Junta de

Andalucía and the grant PID2019-104195G from the Spanish Ministry of Science and Innovation-Agencia Estatal de Investigación/10.13039/501100011033. CABIMER is supported by the regional government of Andalucía (Junta de Andalucía). ADC is funded with FPU fellowships from the Spanish Ministry of Education and RPC is funded with an AECC postdoctoral fellowship. SGP is funded by EMBO Postdoctoral Fellowship ALTF 1039-2021. We also want to thank Paul Guichard and Virginie Hamel (University of Geneva, Department of Cell Biology, Sciences III, Geneva, Switzerland) for their support developing the U-ExM.

Disclosure and competing interest stamen.

The authors declare no actual or perceived conflict of interest.

References:

Al-Dosari MS, Shaheen R, Colak D & Alkuraya FS (2010) Novel CENPJ mutation causes Seckel syndrome. *J Med Genet* 47: 411–414

Alderton GK, Galbiati L, Griffith E, Surinya KH, Neitzel H, Jackson AP, Jeggo PA & O'Driscoll M (2006) Regulation of mitotic entry by microcephalin and its overlap with ATR signalling. *Nat Cell Biol* 8: 725–733

Alves-Cruzeiro JMDC, Nogales-Cadenas R & Pascual-Montano AD (2014) CentrosomeDB: A new generation of the centrosomal proteins database for Human and Drosophila melanogaster. *Nucleic Acids Res* 42: 430–436

Andersen JS, Wilkinson CJ, Mayor T, Mortensen P, Nigg EA & Mann M (2003) Proteomic characterization of the human centrosome by protein correlation profiling. *Nature* 426: 570–574

Arcas A, Fernández-Capetillo O, Cases I & Rojas AM (2014) Emergence and evolutionary analysis of the human DDR network: Implications in comparative genomics and downstream analyses. *Mol Biol Evol* 31: 940–961

Arquint C, Gabryjonczyk AM & Nigg EA (2014) Centrosomes as signalling centres. *Philos Trans R Soc B Biol Sci* 369

Balestra FR, Strnad P, Flückiger I & Gönczy P (2013) Discovering regulators of centriole biogenesis through siRNA-based functional genomics in human cells. *Dev Cell* 25: 555–571

970 Bennardo N, Cheng A, Huang N & Stark JM (2008) Alternative-NHEJ is a
971 mechanistically distinct pathway of mammalian chromosome break repair.
972 *PLoS Genet* 4
973 Bergstrom EN, Huang MN, Mahto U, Barnes M, Stratton MR, Rozen SG &
974 Alexandrov LB (2019) SigProfilerMatrixGenerator: A tool for visualizing and
975 exploring patterns of small mutational events. *BMC Genomics* 20: 1–12
976 Blackford AN & Jackson SP (2017) ATM, ATR, and DNA-PK: The Trinity at the Heart
977 of the DNA Damage Response. *Mol Cell* 66: 801–817
978 Bornens M (2012) The centrosome in cells and organisms. *Science (80-)* 335: 422–
979 426
980 Campbell PJ, Getz G, Korbel JO, Stuart JM, Jennings JL, Stein LD, Perry MD, Nahal-
981 Bose HK, Ouellette BFF, Li CH, *et al* (2020) Pan-cancer analysis of whole
982 genomes. *Nature* 578: 82–93
983 Cejka P (2015) DNA end resection: Nucleases team up with the right partners to
984 initiate homologous recombination. *J Biol Chem* 290: 22931–22938
985 Chang HHY, Pannunzio NR, Adachi N & Lieber MR (2017) Non-homologous DNA
986 end joining and alternative pathways to double-strand break repair. *Nat Rev*
987 *Mol Cell Biol* 18: 495–506
988 Ciccia A & Elledge SJ (2010) The DNA Damage Response: Making It Safe to Play
989 with Knives. *Mol Cell* 40: 179–204
990 Cruz-García A, López-Saavedra A & Huertas P (2014) BRCA1 accelerates CtIP-
991 ediated DNA-end resection. *Cell Rep* 9: 451–459
992 Daly OM, Gaboriau D, Karakaya K, King S, Dantas TJ, Lalor P, Dockery P, Krämer A &
993 Morrison CG (2016) CEP164-null cells generated by genome editing show a
994 ciliation defect with intact DNA repair capacity. *J Cell Sci* 129: 1769–1774
995 Van Dam TJP, Wheway G, Slaats GG, Huynen MA & Giles RH (2013) The SYSCILIA
996 gold standard (SCGSv1) of known ciliary components and its applications
997 within a systems biology consortium. *Cilia* 2: 1–5
998 Dantas TJ, Wang Y, Lalor P, Dockery P & Morrison CG (2011) Defective nucleotide
999 excision repair with normal centrosome structures and functions in the
1000 absence of all vertebrate centrins. *J Cell Biol* 193: 307–318
1001 Dauber A, Lafranchi SH, Maliga Z, Lui JC, Moon JE, McDeed C, Henke K, Zonana J,
1002 Kingman GA, Pers TH, *et al* (2012) Novel microcephalic primordial dwarfism

1003 disorder associated with variants in the centrosomal protein ninein. *J Clin*
1004 *Endocrinol Metab* 97: E2140-51
1005 Evans LT, Anglen T, Scott P, Lukasik K, Loncarek J & Holland AJ (2021) ANKRD26
1006 recruits PIDD1 to centriolar distal appendages to activate the PIDDosome
1007 following centrosome amplification. *EMBO J* 40: 1–18
1008 Fava LL, Schuler F, Sladky V, Haschka MD, Soratroi C, Eiterer L, Demetz E, Weiss G,
1009 Geley S, Nigg EA, *et al* (2017) The PIDDosome activates p53 in response to
1010 supernumerary centrosomes. *Genes Dev* 31: 34–45
1011 Fong CS, Mazo G, Das T, Goodman J, Kim M, O'Rourke BP, Izquierdo D & Tsou MFB
1012 (2016) 53BP1 and USP28 mediate p53- dependent cell cycle arrest in
1013 response to centrosome loss and prolonged mitosis. *Elife* 5: 1–18
1014 Gambarotto D, Zwettler FU, Le Guennec M, Schmidt-Cernohorska M, Fortun D,
1015 Borgers S, Heine J, Schloetel JG, Reuss M, Unser M, *et al* (2019) Imaging
1016 cellular ultrastructures using expansion microscopy (U-ExM). *Nat Methods* 16:
1017 71–74
1018 Gerdes JM, Davis EE & Katsanis N (2009) The Vertebrate Primary Cilium in
1019 Development, Homeostasis, and Disease. *Cell* 137: 32–45
1020 Gönczy P (2015) Centrosomes and cancer: Revisiting a long-standing relationship.
1021 *Nat Rev Cancer* 15: 639–652
1022 Gönczy P & Hatzopoulos GN (2019) Centriole assembly at a glance. *J Cell Sci* 132
1023 Griffith E, Walker S, Martin CA, Vagnarelli P, Stiff T, Vernay B, Sanna N Al, Saggar A,
1024 Hamel B, Earnshaw WC, *et al* (2008) Mutations in pericentrin cause Seckel
1025 syndrome with defective ATR-dependent DNA damage signaling. *Nat Genet*
1026 40: 232–236
1027 Guarguaglini G, Duncan PI, Stierhof YD, Holmström T, Duensing S & Nigg EA (2005)
1028 The forkhead-associated domain protein Cep170 interacts with Polo-like
1029 kinase 1 and serves as a marker for mature centrioles. *Mol Biol Cell* 16: 1095–
1030 107
1031 Le Guennec M, Klena N, Aeschlimann G, Hamel V & Guichard P (2021) Overview of
1032 the centriole architecture. *Curr Opin Struct Biol* 66: 58–65
1033 Hachet V, Canard C & Gönczy P (2007) Centrosomes Promote Timely Mitotic Entry
1034 in C. elegans Embryos. *Dev Cell* 12: 531–541
1035 Hall NA & Hehnly H (2021) A centriole's subdistal appendages: contributions to

1036 cell division, ciliogenesis and differentiation. *Open Biol* 11: 200399
1037 Hauge S, Macurek L & Syljuåsen RG (2019) p21 limits S phase DNA damage caused
1038 by the Wee1 inhibitor MK1775. *Cell Cycle* 18: 834–847
1039 Huertas P (2010) DNA resection in eukaryotes: Deciding how to fix the break. *Nat*
1040 *Struct Mol Biol* 17: 11–16
1041 Islam SMA, Wu Y, Díaz-Gay M, Bergstrom EN, He Y, Barnes M, Vella M, Wang J,
1042 Teague JW, Clapham P, *et al* (2020) Uncovering novel mutational signatures
1043 by de novo extraction with SigProfilerExtractor. *bioRxiv*
1044 Jackson SP & Bartek J (2009) The DNA-damage response in human biology and
1045 disease. *Nature* 461: 1071–1078
1046 Jakobsen L, Vanselow K, Skogs M, Toyoda Y, Lundberg E, Poser I, Falkenby LG,
1047 Bennetzen M, Westendorf J, Nigg EA, *et al* (2011) Novel asymmetrically
1048 localizing components of human centrosomes identified by complementary
1049 proteomics methods. *EMBO J* 30: 1520–1535
1050 Jasin M & Rothstein R (2013) Repair of strand breaks by homologous
1051 recombination. *Cold Spring Harb Perspect Biol* 5
1052 Kalay E, Yigit G, Aslan Y, Brown KE, Pohl E, Bicknell LS, Kayserili H, Li Y, Tüysüz B,
1053 Nürnberg G, *et al* (2011) CEP152 is a genome maintenance protein disrupted
1054 in Seckel syndrome. *Nat Genet* 43: 23–26
1055 Kim J, Lee JE, Heynen-Genel S, Suyama E, Ono K, Lee K, Ideker T, Aza-Blanc P &
1056 Gleeson JG (2010) Functional genomic screen for modulators of ciliogenesis
1057 and cilium length. *Nature* 464: 1048–1051
1058 Lambrus BG, Daggubati V, Uetake Y, Scott PM, Clutario KM, Sluder G & Holland AJ
1059 (2016) A USP28-53BP1-p53-p21 signaling axis arrests growth after
1060 centrosome loss or prolonged mitosis. *J Cell Biol* 214: 143–153
1061 Lambrus BG, Uetake Y, Clutario KM, Daggubati V, Snyder M, Sluder G & Holland AJ
1062 (2015) P53 protects against genome instability following centriole duplication
1063 failure. *J Cell Biol* 210: 63–77
1064 Leidel S, Delattre M, Cerutti L, Baumer K & Gönczy P (2005) SAS-6 defines a
1065 protein family required for centrosome duplication in C. elegans and in human
1066 cells. *Nat Cell Biol* 7: 115–125
1067 Li JB, Gerdes JM, Haycraft CJ, Fan Y, Teslovich TM, May-Simera H, Li H, Blacque OE,
1068 Li L, Leitch CC, *et al* (2004) Comparative genomics identifies a flagellar and

1069 basal body proteome that includes the BBS5 human disease gene. *Cell* 117:
1070 541–552
1071 Livak KJ & Schmittgen TD (2001) Analysis of relative gene expression data using
1072 real-time quantitative PCR and the 2-ΔΔCT method. *Methods* 25: 402–408
1073 López-Saavedra A, Gómez-Cabello D, Domínguez-Sánchez MS, Mejías-Navarro F,
1074 Fernández-Ávila MJ, Dinant C, Martínez-Macías MI, Bartek J & Huertas P
1075 (2016) A genome-wide screening uncovers the role of CCAR2 as an antagonist
1076 of DNA end resection. *Nat Commun* 7
1077 Matsuoka S, Ballif BA, Smogorzewska A, McDonald ER, Hurov KE, Luo J, Bakalarski
1078 CE, Zhao Z, Solimini N, Lerenthal Y, *et al* (2007) ATM and ATR substrate
1079 analysis reveals extensive protein networks responsive to DNA damage.
1080 *Science (80-)* 316: 1160–1166
1081 Meitinger F, Anzola J V., Kaulich M, Richardson A, Stender JD, Benner C, Glass CK,
1082 Dowdy SF, Desai A, Shiau AK, *et al* (2016) 53BP1 and USP28 mediate p53
1083 activation and G1 arrest after centrosome loss or extended mitotic duration. *J*
1084 *Cell Biol* 214: 155–166
1085 Meitinger F, Ohta M, Lee KY, Watanabe S, Davis RL, Anzola J V., Kabeche R, Jenkins
1086 DA, Shiau AK, Desai A, *et al* (2020) TRIM37 controls cancer-specific
1087 vulnerability to PLK4 inhibition. *Nature* 585: 440–446
1088 Michelena J & Altmeyer M (2017) Cell Cycle Resolved Measurements of Poly(ADP-
1089 Ribose) Formation and DNA Damage Signaling by Quantitative Image-Based
1090 Cytometry. In *Methods in Molecular Biology* pp 57–68.
1091 Milanowska K, Krwawicz J, Papaj G, Kosiński J, Poleszak K, Lesiak J, Osińska E,
1092 Rother K & Bujnicki JM (2011) REPAIRtoire-A database of DNA repair
1093 pathways. *Nucleic Acids Res* 39: 788–792
1094 Mönnich M, Borgeskov L, Breslin L, Jakobsen L, Rogowski M, Doganli C, Schrøder
1095 JM, Mogensen JB, Blinkenkjær L, Harder LM, *et al* (2018) CEP128 Localizes to
1096 the Subdistal Appendages of the Mother Centriole and Regulates TGF-β/BMP
1097 Signaling at the Primary Cilium. *Cell Rep* 22: 2584–2592
1098 Moyer TC, Clutario KM, Lambrus BG, Daggubati V & Holland AJ (2015) Binding of
1099 STIL to Plk4 activates kinase activity to promote centriole assembly. *J Cell Biol*
1100 209: 863–878
1101 Mullee LI & Morrison CG (2016) Centrosomes in the DNA damage response—the

1102 hub outside the centre. *Chromosom Res* 24: 35–51
1103 Nabais C, Peneda C & Bettencourt-Dias M (2020) Evolution of centriole assembly.
1104 *Curr Biol* 30: R494–R502
1105 Nigg EA & Raff JW (2009) Centrioles, Centrosomes, and Cilia in Health and Disease.
1106 *Cell* 139: 663–678
1107 O'Driscoll M, Gennery AR, Seidel J, Concannon P & Jeggo PA (2004) An overview of
1108 three new disorders associated with genetic instability: LIG4 syndrome, RS-
1109 SCID and ATR-Seckel syndrome. *DNA Repair (Amst)* 3: 1227–1235
1110 Pierce AJ, Johnson RD, Thompson LH & Jasin M (1999) XRCC3 promotes homology-
1111 directed repair of DNA damage in mammalian cells service XRCC3 promotes
1112 homology-directed repair of DNA damage in mammalian cells. 2633–2638
1113 Portier N, Audhya A, Maddox PS, Green RA, Dammermann A, Desai A & Oegema K
1114 (2007) A Microtubule-Independent Role for Centrosomes and Aurora A in
1115 Nuclear Envelope Breakdown. *Dev Cell* 12: 515–529
1116 Prados-Carvajal R, Rodríguez-Real G, Gutierrez-Pozo G & Huertas P (2021) CtIP-
1117 mediated alternative mRNA splicing fine-tunes the DNA damage response.
1118 *Rna* 27: 303–323
1119 Qvist P, Huertas P, Jimeno S, Nyegaard M, Hassan MJ, Jackson SP & Borglum AD
1120 (2011) CtIP Mutations Cause Seckel and Jawad Syndromes. *PLoS Genet* 7:
1121 e1002310
1122 Ranjha L, Howard SM & Cejka P (2018) Main steps in DNA double-strand break
1123 repair: an introduction to homologous recombination and related processes.
1124 *Chromosoma* 127: 187–214
1125 Shaheen R, Faqeih E, Ansari S, Abdel-Salam G, Al-Hassnan ZN, Al-Shidi T, Alomar R,
1126 Sogaty S & Alkuraya FS (2014) Genomic analysis of primordial dwarfism
1127 reveals novel disease genes. *Genome Res* 24: 291–299
1128 Sir J-H, Barr AR, Nicholas AK, Carvalho OP, Khurshid M, Sossick A, Reichelt S,
1129 D'Santos C, Woods CG & Gergely F (2011) A primary microcephaly protein
1130 complex forms a ring around parental centrioles. *Nat Genet* 43: 1147–1153
1131 Sir JH, Pütz M, Daly O, Morrison CG, Dunning M, Kilmartin J V. & Gergely F (2013)
1132 Loss of centrioles causes chromosomal instability in vertebrate somatic cells. *J*
1133 *Cell Biol* 203: 747–756
1134 Sivasubramaniam S, Sun X, Pan YR, Wang S & Lee EYHP (2008) Cep164 is a

1135 mediator protein required for the maintenance of genomic stability through
1136 modulation of MDC1, RPA, and CHK1. *Genes Dev* 22: 587–600
1137 Symington LS (2016) Mechanism and regulation of DNA end resection in
1138 eukaryotes. *Crit Rev Biochem Mol Biol* 51: 195–212
1139 Tate JG, Bamford S, Jubb HC, Sondka Z, Beare DM, Bindal N, Boutselakis H, Cole CG,
1140 Creatore C, Dawson E, *et al* (2019) COSMIC: The Catalogue Of Somatic
1141 Mutations In Cancer. *Nucleic Acids Res* 47: D941–D947
1142 Tubbs A & Nussenzweig A (2017) Endogenous DNA Damage as a Source of
1143 Genomic Instability in Cancer. *Cell* 168: 644–656
1144 Wang WJ, Acehan D, Kao CH, Jane WN, Uryu K & Tsou MFB (2015) De novo
1145 centriole formation in human cells is error-prone and does not require SAS-6
1146 self-assembly. *Elife* 4: 1–13
1147 Wong YL, Anzola J V., Davis RL, Yoon M, Motamedi A, Kroll A, Seo CP, Hsia JE, Kim
1148 SK, Mitchell JW, *et al* (2015) Reversible centriole depletion with an inhibitor of
1149 Polo-like kinase 4. *Science (80-)* 348: 1155–1160
1150 Yeow ZY, Lambrus BG, Marlow R, Zhan KH, Durin MA, Evans LT, Scott PM, Phan T,
1151 Park E, Ruiz LA, *et al* (2020) Targeting TRIM37-driven centrosome
1152 dysfunction in 17q23-amplified breast cancer. *Nature* 585: 447–452
1153
1154
1155 **Figure Legends:**
1156 **Figure 1: Centrosomes control the balance between repair mechanisms. A**,
1157 Homologous recombination was assessed in U2OS cells bearing the DR-GFP
1158 reporter in cells lacking centrosomes upon the treatment with centrinone for 7
1159 days or mock-treated with DMSO. A schematic representation of the reporter and
1160 the recombination event that renders the appearance of a functional GFP gene is
1161 shown on the left side. Within the BFP positive cell population, i.e. cells transfected
1162 with I-Sce-I containing viral particles, the percentage of GFP positive cells, i.e. cells
1163 that have undergone repair by HR after induction with the nuclease I-SceI, was
1164 normalized to the DMSO control taken as 1. **B**, Same as A but in cells harboring the
1165 NHEJ reporter EJ5-GFP. **C**, U2OS cells treated for 7 days with centrinone or DMSO,
1166 as indicated, were irradiated with 10 Gy and 1 hour later prepared for
1167 immunofluorescence using an anti-RPA antibody as described in the methods

1168 section. The number of RPA foci per cell for at least 200 cells per condition was
1169 quantified automatically using FIJI software and plotted. One representative
1170 experiment out of three performed with similar results is shown. (top).
1171 Representative images are shown (bottom). Scale bar in white represents 7 μm. **D**,
1172 Same as C, but using an antibody against BRCA1. **E**, Same as C, but using an anti-
1173 RAD51 antibody. **F**, U2OS cells were treated 7 days with centrinone or DMSO as
1174 control before a 30-minutes pulse-labeled with EdU. Afterward, cells were
1175 irradiated (10 Gy) and incubated for one hour. Click-it reaction and
1176 immunostaining against RPA was carried out as described in the methods section.
1177 Automated multichannel wide-field microscopy for quantitative image-based
1178 cytometry (QIBC) was performed. Single-cell data for more than 5000 cells is
1179 depicted as scatter plots showing DNA content (DAPI intensity) and EdU
1180 incorporation during S phase (EdU intensity). Correlatively, RPA foci was
1181 measured for each cell. Cells with more than 15 RPA foci are classified as positive
1182 (labelled in red). **G**, Quantification of RPA foci positive cells regarding cell cycle
1183 status from three different experiments analyzed as described in F. **H**,
1184 Representative images of F and G are shown. Scale bar in white represents 7 μm. In
1185 A, B and G the average and standard deviation of three independent experiments is
1186 shown. The statistical significance was calculated using a Student´s t-test. p values
1187 are represented with one ($p < 0.05$), two ($p < 0.01$), three ($p < 0.001$) or four ($p <$
1188 0.0001) asterisks. Non statistical significance is labeled ns.
1189
1190 **Figure 2: CEP170 and the Subdistal appendages regulate DNA end resection.**
1191 **A**, Venn diagram showing the overlapping of genes found both in DDR screenings
1192 and centrosome related screening, as described in the main text and the method
1193 section. **B**, Schematics of the centrioles showing the Distal and Subdistal
1194 appendages (DA and SDA, respectively). The inset shows the molecular
1195 architecture of the SDA. **C**, Cells transfected with siRNAs against the indicated
1196 proteins or a siRNA control (siNT) and the number of RPA foci per cell for at least
1197 200 cells per condition was quantified automatically using FIJI software and
1198 plotted. One representative experiment out of three performed with similar results
1199 is shown (top). Representative images are shown (bottom). Scale bar in white
1200 represents 7 μm. **D**, the same samples used in C were used to immunodetect

1201 CEP170 at centrioles. Intensity of individual cells is plotted (top) in cells depleted
1202 for the indicated factors. Representative images of each condition are shown on
1203 the bottom side. For each condition, insets of centrosomes labelled by either
1204 CEP170 or γ-tubulin are shown. **E**, linear correlation between RPA foci and CEP170
1205 intensity. For each condition, the average calculated in C and D was used in the
1206 plot. The R^2, linear correlation and mathematical formula are shown. **F**, cells
1207 harboring a plasmid expressing an siRNA-resistant GFP-tagged CEP170 or an
1208 empty vector were transfected with siRNAs against CEP170 or a control sequence
1209 (siNT). Then, cells were treated with IR and the number of RPA foci per cell was
1210 quantified as in C (top). Representative images are shown (bottom). **G**, Same as C
1211 but in RPE-1 cells with partial knock out of CEP170 (top). Representative images
1212 are shown (bottom). In C, D, F, and G, the statistical significance was calculated
1213 using a Student´s t-test. p values are represented with one ($p < 0.05$), two ($p <$
1214 0.01), three ($p < 0.001$) or four ($p < 0.0001$) asterisks. Non statistical significance is
1215 labeled ns.
1216
1217 **Figure 3: CEP170 phosphorylation at centrosomes is required for resection.**
1218 **A**, Cells were treated with centrinone or the vehicle DMSO and transfected with the
1219 indicated siRNAs. The number of RPA foci per cell for at least 200 cells per
1220 condition was quantified automatically using FIJI software and plotted. One
1221 representative experiment out of three performed with similar results is shown
1222 (left). Representative images are shown (right). Scale bar in white represents 7
1223 μm. Statistical significance was calculated using a two-way ANOVA. **B**, HR was
1224 studied as indicated in figure 1A in cells bearing the DR-GFP reporter depleted for
1225 the indicated factors. **C**, Same as B, but using cells harboring the NHEJ reporter EJ5-
1226 GFP. **D**, The number of BRCA1 foci per cell for at least 200 cells transfected with an
1227 siRNA against CEP170 or a siRNA control was quantified automatically using FIJI
1228 software and plotted. One representative experiment out of three performed with
1229 similar results is shown (left). Representative image on the right side. **E**, Same as D
1230 but using an antibody against RAD51 (left). Representative images on the right
1231 side. **F**, Same as D but using an antibody against RIF1 (top). Representative images
1232 at the bottom. **G**, Ultraextructure expansion microscopy (U-ExM) images of U2OS
1233 expressing GFP, GFP-CEP170 WT, GFP-CEP170 S637A or GFP-CEP170 S637D.

1234 Images show one representative top view (top panels) and side view (bottom
1235 panels). Cells were co-immunostained against alpha and beta tubulin and
1236 endogenous CEP170 or GFP as indicated. Orange numbers label the nine SDAs.
1237 Orange arrows point to subdistal appendage localization and white arrows to
1238 centriole proximal localization of CEP170 variants. Scale bar 500 nm. **H**, same as A
1239 but in cells stably expressing the indicated CEP170 variant tagged with GFP or the
1240 control GFP plasmid and transfected with siCEP170 or a control sequence (left).
1241 Representative images on the right side. In B and C the average and standard
1242 deviation of three independent experiments is shown. A-F and H the statistical
1243 significance was calculated using a Student´s t-test. p values are represented with
1244 one ($p < 0.05$), two ($p < 0.01$), three ($p < 0.001$) or four ($p < 0.0001$) asterisks. Non
1245 statistical significance is labeled ns.
1246
1247
1248
1249 **Figure 4: Centrosomes or CEP170 loss hyper-sensitize to treatment with DNA**
1250 **damaging agents. A**, RPE-1 cells knocked out for p53 and heterozygous for
1251 CEP170 (red) or a control RPE-1 p53 KO cells (blue) were exposed to the indicated
1252 doses of ionizing radiation. Cell survival was analyzed as described in the methods
1253 section using a clonogenic assay. Statistical significance was calculated using a
1254 two-way ANOVA. **B**, Same as A but treating cells with the indicated doses of NCS. **C**,
1255 Same as A but in cells treated with the indicated doses of CPT. **D**, Same as A but in
1256 cells treated with the indicated doses of VP-16. **E**, Same as A but in RPE p53-/- cells
1257 treated with centrinone (red) or DMSO (blue) for 7 days prior the treatment with
1258 ionizing radiation. **F**, Same as E but in cells treated with the indicated doses of NCS.
1259 **G,** Same as E but in cells treated with the indicated doses of CPT. **H**, Same as E but
1260 in cells treated with the indicated doses of VP-16. **I**, U2OS cells expressing GFP or
1261 GFP-CEP170 and transfected with siRNA against CEP170 or non-target sequence
1262 were exposed to ionizing irradiation or mock treated. Cell survival was analyzed as
1263 in A. Statistical significance was calculated using a two-way ANOVA. p values are
1264 represented with one ($p < 0.05$), two ($p < 0.01$), three ($p < 0.001$) or four ($p <$
1265 0.0001) asterisks. Non statistical significance is labeled ns. **J**, Representative
1266 scanned images of clonogenic assay represented in I. Data shown in all panels are

1267 the average of three biological independent experiments each of them performed
1268 in three technical replicates.
1269
1270 **Figure 5: CEP170 levels modulate the mutational signature in cancer**
1271 **samples. A**, CEP170 levels in tumor samples (red) and the equivalent healthy
1272 tissue (black), studied as indicated in the methods section. Tumor acronyms are:
1273 ACC Adrenocortical carcinoma; BLCA Bladder urothelial carcinoma; BRCA Breast
1274 invasive carcinoma; CESC Cervical squamous cell carcinoma and endocervical
1275 adenocarcinoma; CHOL Cholangiocarcinoma; COAD Colon adenocarcinoma; DLBC
1276 Lymphoid neoplasm diffuse large B-cell lymphoma; ESCA Esophageal carcinoma;
1277 GBM Glioblastoma multiforme; HNSC Head and neck squamous cell carcinoma;
1278 KICH Kidney chromophobe; KIRC Kidney renal clear cell carcinoma; KIRP Kidney
1279 renal papillary cell carcinoma; LAML Acute myeloid leukemia; LGG Brain lower
1280 grade glioma; LHIC Liver hepatocellular carcinoma; LUAD Lung adenocarcinoma;
1281 LUSC Lung squamous cell carcinoma; OV Ovarian serous cystadenocarcinoma;
1282 PAAD Pancreatic adenocarcinoma; PCPG Pheochromocytoma and Paraganglioma;
1283 PRAD Prostate adenocarcinoma; READ Rectum adenocarcinoma; SARC Sarcoma;
1284 SKCM Skin cutaneous melanoma; STAD Stomach adenocarcinoma; TGCT Testicular
1285 germ cell tumors; THCA Thyroid carcinoma; THYM Thymoma; UCEC Uterine
1286 corpus endometrial carcinoma; UCS Uterine carcinosarcoma. **B**, Cancer samples
1287 from PCAWG database containing mutation and CEP170 expression data were
1288 analyzed using SigProfiler to determine the number of significant signatures that
1289 could be analyzed in the dataset. The average stability and Mean Sample Cosine
1290 were plotted, and the number of optimal signatures was defined as 16. For other
1291 details, see the methods section. **C-R**, Each of the 16 optimal mutational signatures
1292 were analyzed in samples at the lower quartile of CEP170 (low) or at the highest
1293 (high). The number of mutations in each sample associated to each signature was
1294 plotted. The average is shown. Statistical significance was calculated using a
1295 Wilcoxon test, and the p-value is shown on top of the graph. The assigned name of
1296 the signature is shown on top. The name of those signatures that show statistically
1297 significant changes between samples with high and low expression of CEP170 is
1298 written in red. For those signatures associated with a known etiology according to
1299 the COSMIC database, this is depicted between the name and the p-value.

1300

1301 **Figure 6: CEP170 levels predict the prognosis of cancer patients.** Survival data
1302 in different cancer types with different CEP170 expression were collected from the
1303 web-based tool GEPIA. Samples were split in two categories, the ones with an
1304 expression above the median (high; red lines) or below the median (low; blue
1305 lines). Overall survival of each category in each cancer type were plotted in Kaplan-
1306 Meyer graphs. Statistical significance was calculated using a Log-rank (Mantel-Cox)
1307 test and the p values are included. Tumor types: **A**, ACC Adrenocortical carcinoma.
1308 **B**, CESC Cervical squamous cell carcinoma and endocervical adenocarcinoma. **C**,
1309 COAD Colon adenocarcinoma. **D**, DLBC Lymphoid neoplasm diffuse large B-cell
1310 lymphoma. **E**, KICH Kidney chromophobe. **F**, KIRP Kidney renal papillary cell
1311 carcinoma. **G**, LHIC Liver hepatocellular carcinoma. **H**, LUSC Lung squamous cell
1312 carcinoma; **I**, MESO Mesothelioma. **J**, SARC Sarcoma. **K**, STAD Stomach
1313 adenocarcinoma. **L**, THCA Thyroid carcinoma.

1314

1315 **Expanded View Figure Legends:**

1316

1317 **Figure EV 1: Lack of centrioles affect DNA repair by homologous**
1318 **recombination. A-B**, U2OS cells were treated with 125nM of centrinone, or DMSO
1319 as a control, for 24 h (A) or 7 days (B). Then, the presence of centrosomes was
1320 immunodetected using an antibody against the centriolar proteins γ-tubulin and
1321 CP110. The number of cells without centrioles was counted and plotted. **C,** U2OS
1322 cells treated for 7 days with centrinone or DMSO, as indicated, were exposed to
1323 Camptothecin 1μM for 1 h and prepared for immunofluorescence using an anti-
1324 RPA antibody as described in the methods section. The number of RPA foci per cell
1325 for at least 200 cells per condition was quantified automatically using FIJI software
1326 and plotted. One representative experiment out of three performed with similar
1327 results is shown. **D**, RPE-1 cells treated for 7 days with centrinone or DMSO, as
1328 indicated, were irradiated with 10 Gy and 1 hour later prepared for
1329 immunofluorescence using an anti-RPA antibody as described in the methods
1330 section. The number of RPA foci per cell was calculated as in C. **E**, As in D, but in
1331 U2OS cells treated for 24h with centrinone or DMSO. **F**, As in D, but in p53 KO or
1332 p53 KO HsSAS-6 KO RPE-1 cells **G**, U2OS cells transfected with a plasmid

1333 harboring a mCherry-tagged PLK4, or an empty vector as a control, were grown for
1334 3 days. Then, the number of centrosomes was immunodetected using an antibody
1335 against the centriolar proteins γ-tubulin and CP110. The number of cells with more
1336 than four centrioles was counted and plotted. **H**, Same as Figure 1A, but in cells
1337 overexpressing or not PLK4. **I**, Same as Figure 1B, but in cells overexpressing or
1338 not PLK4. **J**, U2OS cells treated for 7 days with centrinone or DMSO, as indicated,
1339 were prepared for immunofluorescence using an anti-γH2AX antibody as
1340 described in the methods section. The number of γH2AX foci per cell for at least
1341 200 cells per condition was quantified automatically using FIJI software and
1342 plotted. One representative experiment out of three performed with similar results
1343 is shown. **K**, DSB repair kinetic using γH2AX as a proxy. U2OS cells exposed to
1344 centrinone or DMSO as a control for 7 days were irradiated (2 Gy). Samples were
1345 collected at the indicated time points and γH2AX was immunodetected using a
1346 specific antibody as described in the method section. NI indicates a non-irradiated
1347 sample taken just before irradiation. The number of γH2AX foci was scored and
1348 plotted. **L**, Same as figure 1C, but using an antibody against the NHEJ factor RIF1.
1349 **M**, Same as figure 1C, but in cells treated with Taxol, Nocodazol or DMSO. **N**, Cell
1350 cycle distribution of samples treated for 7 days with centrinone or DMSO, as
1351 indicated. **O**, U2OS cells treated for 7 days with centrinone or DMSO, as indicated,
1352 were fixed and the percentage of mitotic cells was quantified based on DAPI
1353 staining. At least 400 cells were quantified per condition. **P**, Same as O but cells
1354 were immunostained with an antibody against phospho-H3S10. At least 400 cells
1355 were scored per condition and the percentage of phospho-H3S10 positive cells was
1356 quantified. **Q**, Cell viability of U2OS cells treated for 7 days with centrinone or
1357 DMSO was quantified by Trypan Blue staining and plotted. **R-T**, Same as Figure 1C-
1358 E but using Saos-2 cells. **U-V**, Same as Figure 1C-E but using RPE-1 p53 KO cells. **X-**
1359 **Z**, Same as Figure 1C-E but using RPE-1 p21 KO cells. **A, B, G-I, K, O-Q**, the average
1360 and standard deviation of three independent experiments is shown. The statistical
1361 significance was calculated using a Student´s t-test. p values are represented with
1362 one ($p < 0.05$), two ($p < 0.01$), three ($p < 0.001$) or four ($p < 0.0001$) asterisks. Non
1363 statistical significance is labeled ns.
1364

1365 **Figure EV 2: Identification of the subdistal appendages as involved in HR**
1366 **regulation. A**, Pipeline for identification of candidate genes involved in the
1367 connection between the centrosome and the DDR. **B**, U2OS cells were transfected
1368 with the indicated siRNAs and 48 h later, protein samples were prepared, resolved
1369 in SDS-PAGE and blotted with the indicated antibodies. **C**, U2OS cells were
1370 transfected with the indicated siRNAs. 48 h later, total RNA was isolated and the
1371 levels of the Ndel1 RNA was calculated using Q-PCR. The levels were normalized to
1372 the sample transfected with a control siRNA, taken as one. The average and
1373 standard deviation of three experiments is plotted. Statistical significance was
1374 calculated using a Student's t-test. **D**, Same as C but in cells transfected with an
1375 siRNA against CEP128 and using Q-PCR primers against the mRNA for this protein.
1376 **E**, same as Figure 2D but for RPE-1 CEP128 KO or RPE-1 control cells. **F**, same as
1377 Figure 1C but for RPE-1 CEP128 KO or RPE-1 control cells. **G**, protein samples were
1378 prepared from cells treated as in Figure 2F, resolved in SDS-PAGE and blotted with
1379 the indicated antibodies. **H**, same as Figure EV1C but in CEP170 siRNA depleted or
1380 siRNA control cells. **I and J**, same as in Figure EV1J but for CEP170 siRNA depleted
1381 or siRNA control cells stained with anti-RPA antibodies (I) or γH2AX antibodies (J).
1382 **K**, protein samples were prepared from U2OS CEP170 heterozygous KO clones,
1383 resolved in SDS-PAGE and blotted with the indicated antibodies. **C and D**, the
1384 average and standard deviation of three independent experiments is shown. The
1385 statistical significance was calculated using a Student´s t-test. p values are
1386 represented with one ($p < 0.05$), two ($p < 0.01$), three ($p < 0.001$) or four ($p <$
1387 0.0001) asterisks. Non statistical significance is labeled ns.
1388
1389
1390 **Figure EV 3: CEP170 in response to DNA damage. A**, U2OS cells stably
1391 expressing a GFP-CEP170 construct were irradiated (10 Gy, plus sign) or not
1392 (minus sign). Protein samples were prepared 1 h later by nuclear fractionation as
1393 described in the methods section. Samples were resolved in SDS-PAGE and blotted
1394 with the indicated antibodies. Size ladder marker is shown on the right side. A
1395 representative image of three independent experiments is shown. **B and C**, same
1396 as Figure 1 D and E but for RPE-1 CEP128 KO or RPE-1 control cells. **D**, Total levels
1397 of endogenous CEP170 were immunodetected in protein samples from U2OS cells

1398 irradiated (10Gy, +IR) or not (-IR) resolved in SDS-PAGE using an antibody against
1399 this protein. Size ladder marker is shown on the right side. A representative image
1400 of four independent experiments is shown on the top, and the average and
1401 standard deviation of the quantification of the western blots at the bottom. **E**,
1402 alignment of human CEP170 sequence flanking Serine-637 (red box) with the
1403 homologous sequences from the indicated vertebrates. **F**, protein samples were
1404 prepared from cells treated as in Figure 3H, resolved in SDS-PAGE and blotted with
1405 the indicated antibodies. **G**, Same as in Figure 3G but examples of ectopic
1406 centrosomal localization of GFP tagged CEP170 WT and mutant versions. **H**, Same
1407 as Figure 3H, but in cells pretreated for 1 hour with inhibitors against ATM (ATMi,
1408 white bars), ATR (ATRi, grey bars) or DMSO as a control (left). Representative
1409 images are shown on the right. **I**, Same as Figure 1C but in cells treated with
1410 centrinone or DMSO and stably expressing the indicated GFP constructs. The
1411 statistical significance was calculated using a Student´s t-test. p values are
1412 represented with one ($p < 0.05$), two ($p < 0.01$), three ($p < 0.001$) or four ($p <$
1413 0.0001) asterisks. Non statistical significance is labeled ns.
1414
1415 **Figure EV 4: Centrosomes or CEP170 loss hyper-sensitize to treatment with**
1416 **DNA damaging agents.**
1417 Representative images of clonogenic assays shown in Figure 4A-H
1418
1419 **Figure EV 5: Mutational signatures analyzed in tumor samples with low or**
1420 **high expression of CEP170. A**, for each signature analyzed, the distribution of
1421 single base substitution considering the previous and following base is shown.
1422 Each signature presents a unique profile of mutations. **B**, same as in Figure 5I but
1423 for samples at the lower quartile (low) or at the highest (high) of the indicated
1424 centriolar subdistal appendages proteins.
1425
1426

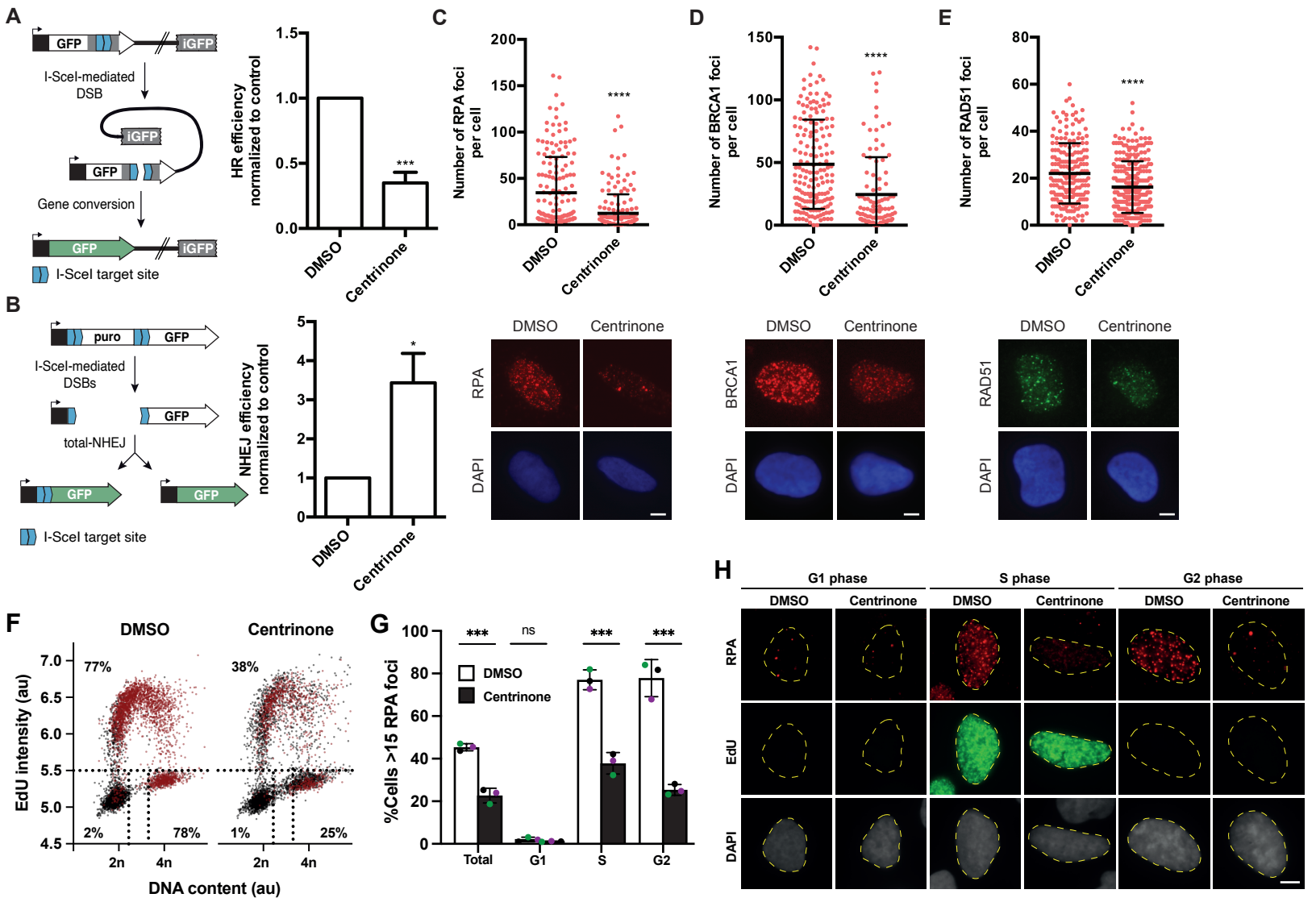

Rodriguez-Real Figure 1

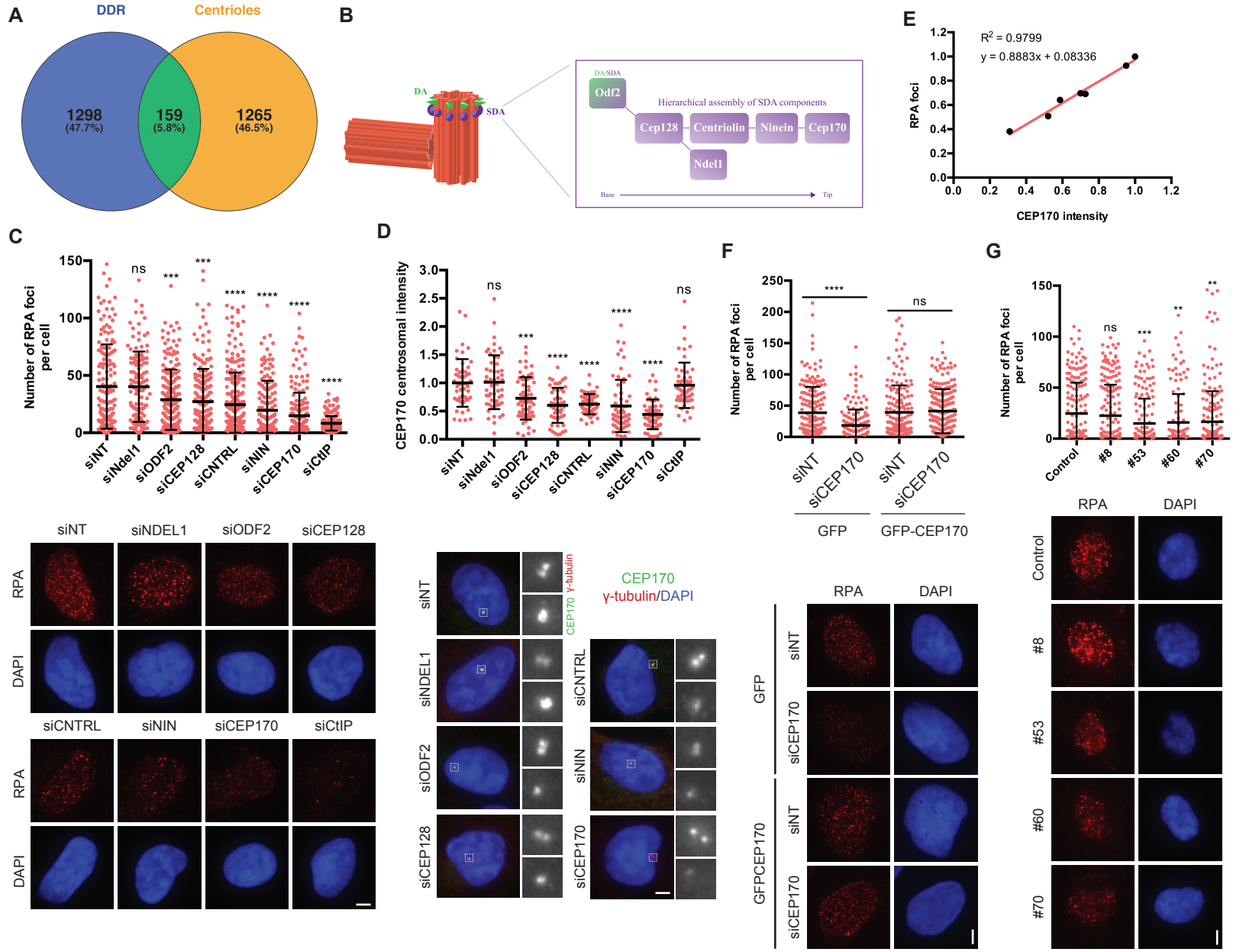

Rodriguez-Real Figure 2

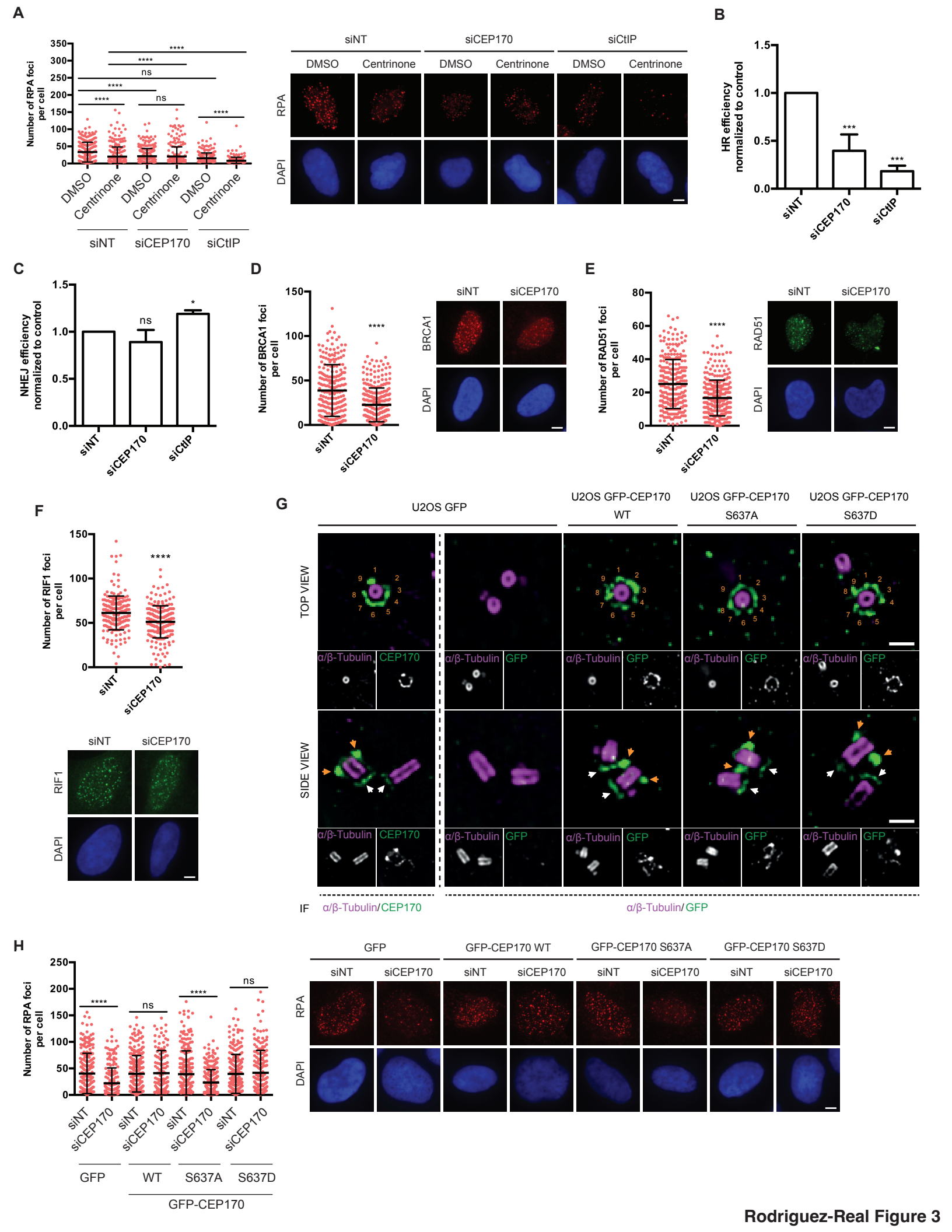

Rodriguez-Real Figure 3

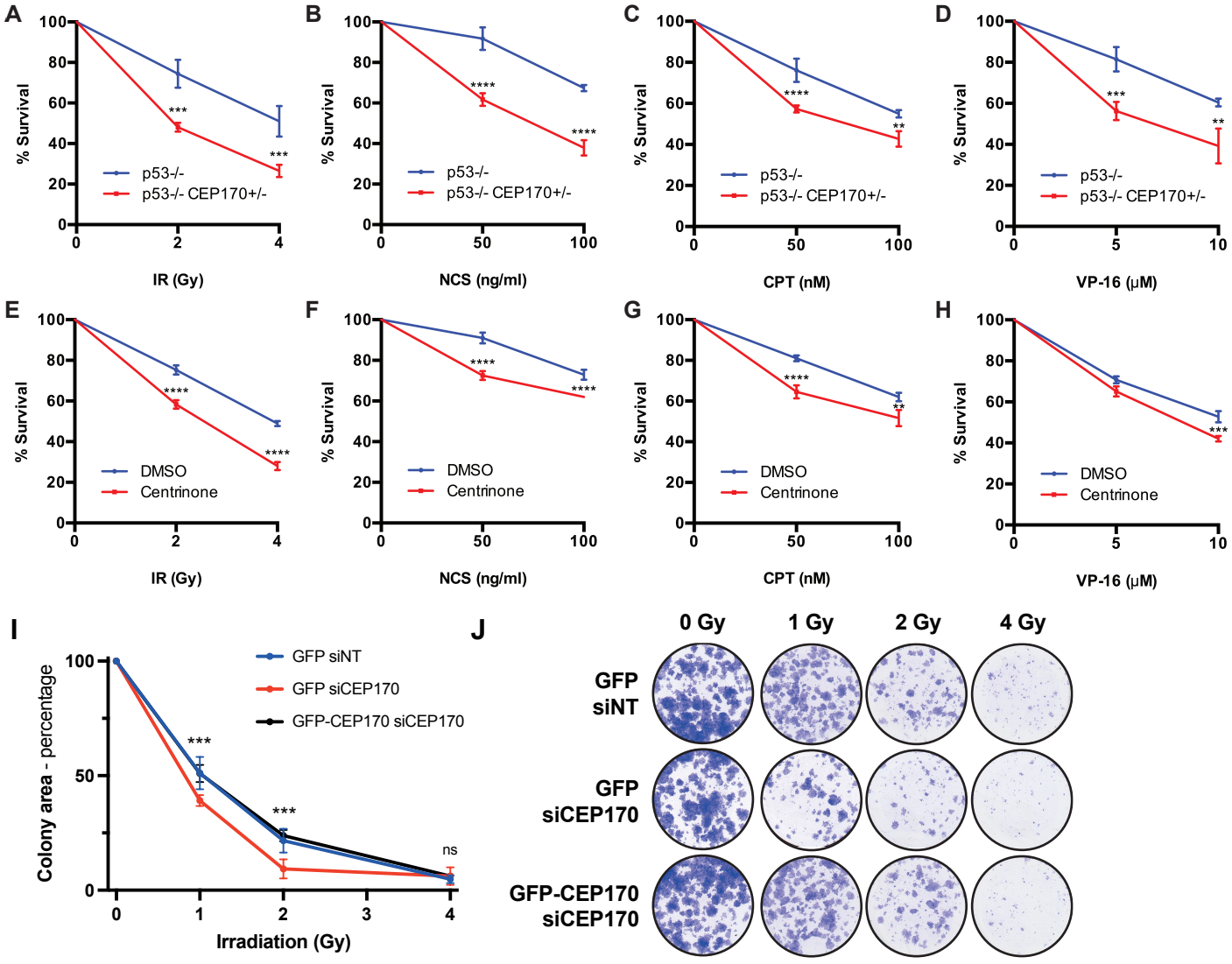

Rodriguez-Real Figure 4

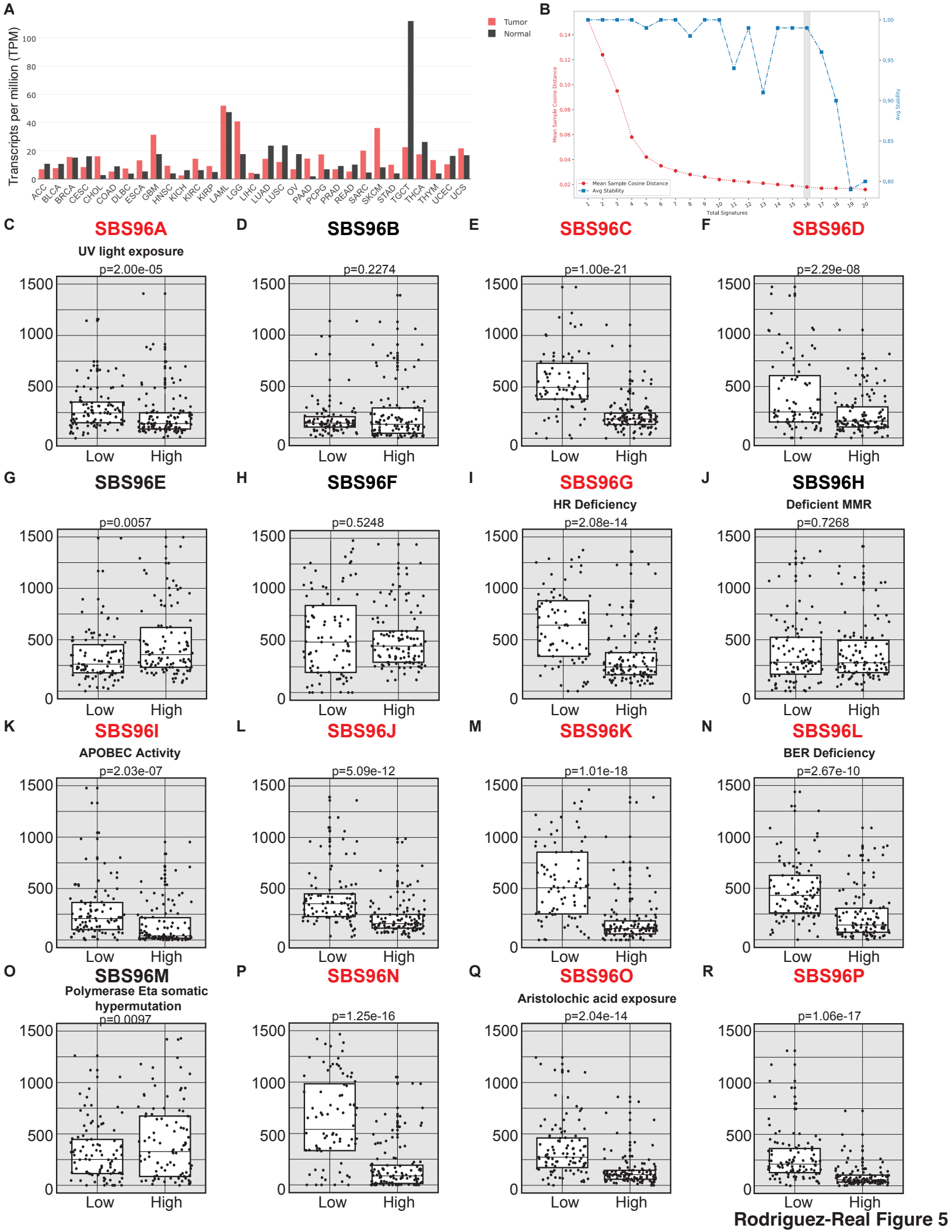

Rodriguez-Real Figure 5

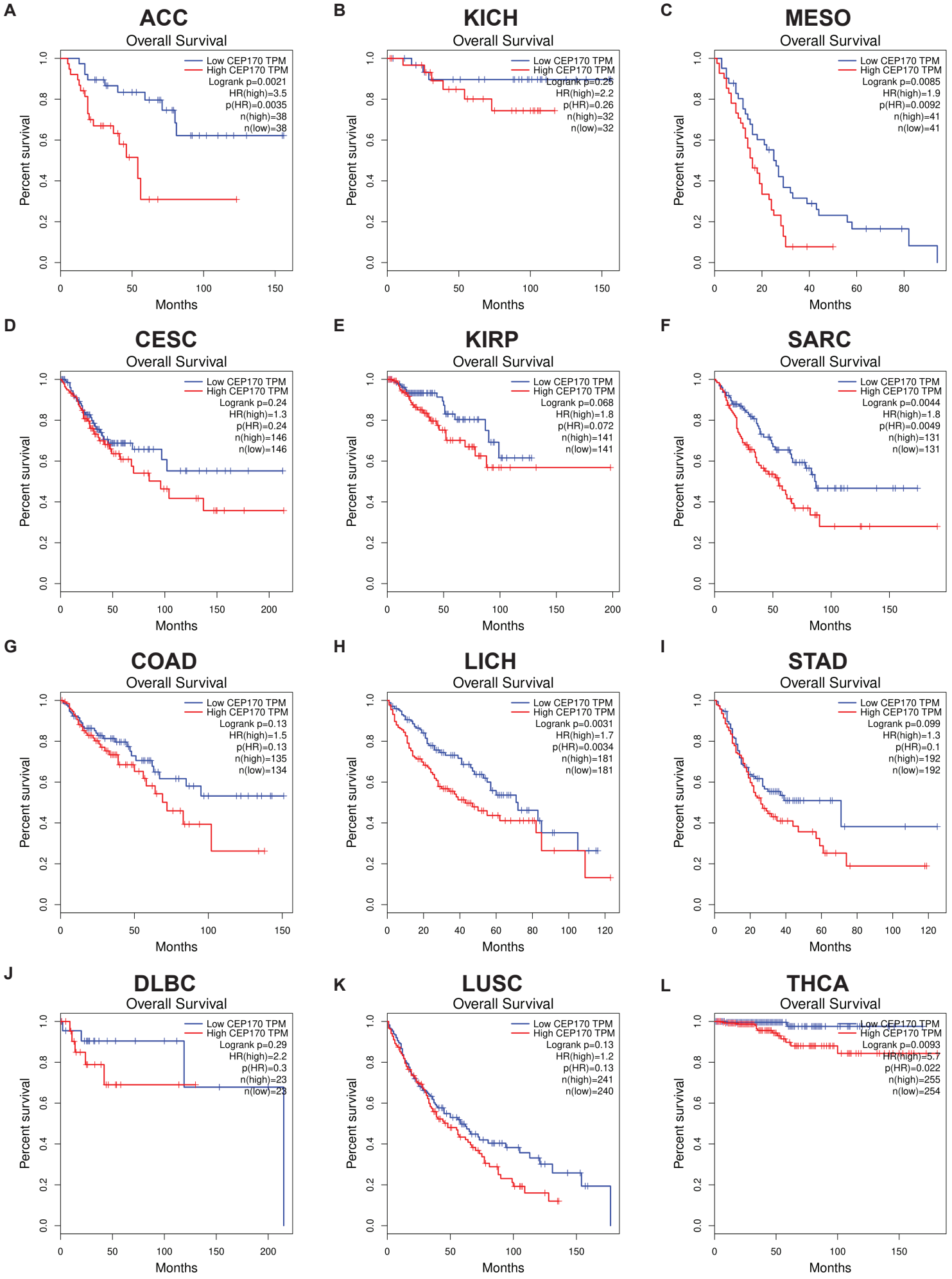

Rodriguez-Real Figure 6